

Provided for non-commercial research and education use.
Not for reproduction, distribution or commercial use.



This article appeared in a journal published by Elsevier. The attached copy is furnished to the author for internal non-commercial research and education use, including for instruction at the authors institution and sharing with colleagues.

Other uses, including reproduction and distribution, or selling or licensing copies, or posting to personal, institutional or third party websites are prohibited.

In most cases authors are permitted to post their version of the article (e.g. in Word or Tex form) to their personal website or institutional repository. Authors requiring further information regarding Elsevier's archiving and manuscript policies are encouraged to visit:

<http://www.elsevier.com/copyright>



Contents lists available at ScienceDirect

Quaternary Science Reviews

journal homepage: www.elsevier.com/locate/quascirev

Millennial-scale variations in hydrography and biogeochemistry in the Eastern Equatorial Pacific over the last 100 kyr

Nathalie Dubois^{a,*}, Markus Kienast^a, Stephanie Kienast^a, Claire Normandeau^a, Stephen E. Calvert^b, Timothy D. Herbert^c, Alan Mix^d

^a Department of Oceanography, Dalhousie University, 1355 Oxford Street, Halifax, Nova Scotia, Canada B3H 4J1

^b Earth and Ocean Sciences Department, University of British Columbia, Vancouver, British Columbia, Canada

^c Department of Geological Sciences, Brown University, Providence, RI, USA

^d College of Oceanic and Atmospheric Sciences, Oregon State University, Corvallis, OR, USA

ARTICLE INFO

Article history:

Received 5 May 2010

Received in revised form

15 October 2010

Accepted 15 October 2010

ABSTRACT

In this study, we use records of nitrogen isotope ratios ($\delta^{15}\text{N}$), UK'37 temperature estimates, organic carbon and opal percentages from high-resolution sediment cores located in the eastern equatorial Pacific (EEP) to explore the mechanisms linking millennial-scale changes in low-latitude sea surface temperature, water column denitrification and surface productivity to the timing of northern or southern polar climate during the last 100,000 yr. Our results support a hypothesis that the Southern Hemisphere, and its connection to the low latitudes via shallow subsurface ocean circulation, has a primary influence on the biogeochemistry of the EEP. In addition, our results suggest that, during the last glacial stage, denitrification rates fluctuated on millennial timescales in response to water-column ventilation rather than upstream oxidant demand in intermediate-depth waters.

However, due to the poor age constraints available for Marine Isotopic Stage (MIS) 3, the EEP sedimentary data presented here could support two conflicting mechanisms, one driven by enhanced intermediate overturning circulation in the Southern Ocean during Heinrich Events/Antarctic Warm Events, implying that subsurface flow rates control thermocline ventilation, and a second one consistent with more sluggish intermediate circulation during Antarctic Warm Events and giving a central role to the temperature control on oxygen solubility in Southern Ocean surface waters.

© 2010 Elsevier Ltd. All rights reserved.

1. Introduction

The eastern equatorial Pacific (EEP) is a critical region for understanding past global climate change. This region is characterized by the presence of a shallow and steep thermocline, which leads to a strong coupling between the atmosphere and surface ocean (Mitchell and Wallace, 1992). As a result, it undergoes fast dynamic adjustments and remarkably large sea surface temperature (SST) changes. The temperature of the EEP Cold Tongue serves as a diagnostic of trade wind strength, thermocline depth, upwelling of cold subsurface waters, and advection of waters off the eastern boundary. The impacts of the El-Niño/Southern Oscillation in this region are responsible for the earth's greatest interannual climatic variability.

The EEP is also a key area for globally important biogeochemical cycles. For example, it is an important oceanic source of carbon dioxide (CO_2) to the atmosphere on annual and decadal time scales (Takahashi et al., 2002), and is responsible for up to 18–56% of global oceanic new (export) productivity (Chavez and Barber, 1987). Because of this high production and strong stratification of the upper ocean, as well as the relative isolation of subsurface water masses, the ocean's two largest subsurface oxygen minimum zones (OMZ) are located north and south of the equator in the eastern tropical Pacific (Fig. 1a). Suboxic conditions give rise to water-column and sedimentary denitrification, the bacterial reduction of nitrate under low oxygen conditions, which also provides a significant source of nitrous oxide (N_2O), a powerful greenhouse gas, to the atmosphere (Nevison et al., 1995).

In addition, the EEP may record a climate feature that contributes to the conditioning of the background state for the formation of North Atlantic Deep Water (NADW) (Zaucker et al., 1994; Benway and Mix, 2004): North of the equator, this region receives a significant amount of Atlantic-derived freshwater through cross-isthmus

* Corresponding author. Tel.: +1 902 402 4195; fax: +1 902 494 3877.
E-mail address: nathalie.dubois@dal.ca (N. Dubois).

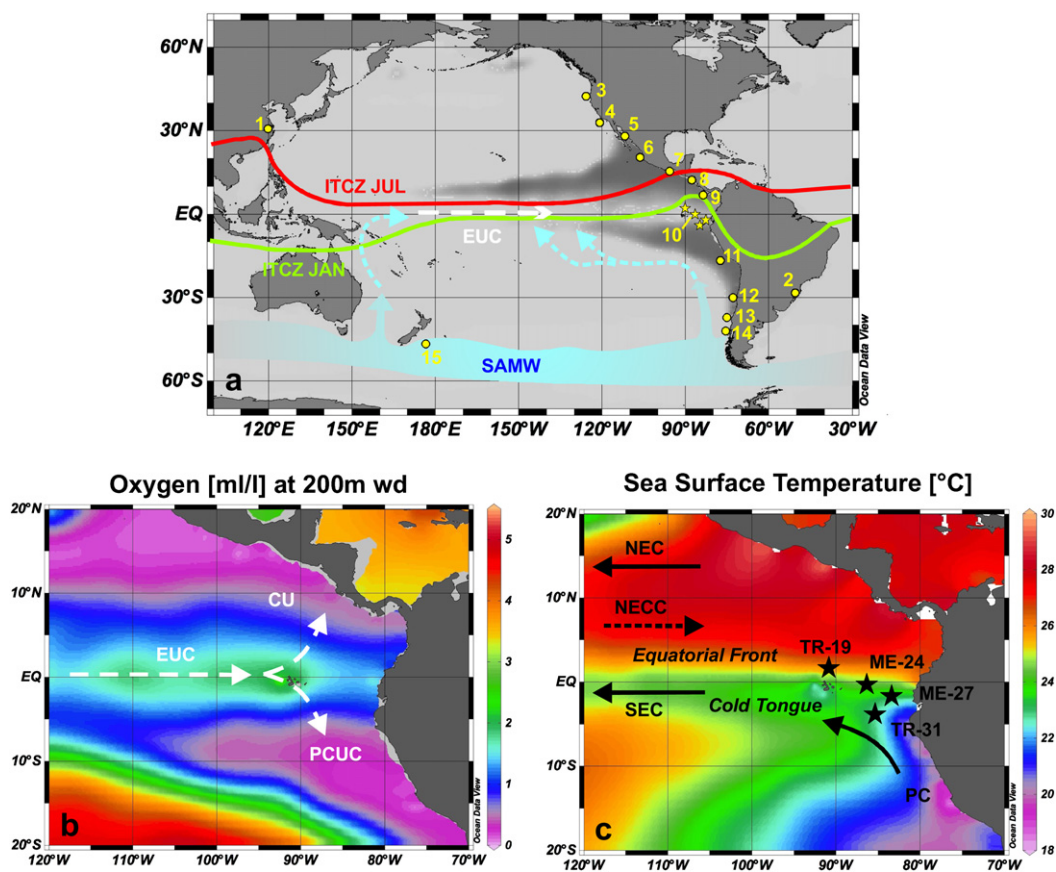


Fig. 1. (a) Schematic illustration of the oceanic and atmospheric processes discussed in this paper. The colored lines show the location of the Inter-Tropical Convergence Zone (ITCZ), in red for present-day July, in green for present-day January. The grey shaded area shows the extent of the oxygen minimum zones at 200 m water depth. The light blue area shows the formation zone of Sub-Antarctic Mode Water (SAMW), while the blue dotted arrows illustrate possible pathways for the “tunneling” of intermediate waters. Yellow stars represent the core locations, as shown in (c), as well as cores used in Robinson et al. (2009). Yellow dots show the locations of the paleoclimatic and paleoceanographic records discussed in the text: (1) Hulu Cave speleothem records (as discussed in Toggweiler and Lea, 2010), (2) Caverna Botuvera speleothem records (Wang et al., 2007), (3) Oregon margin (Kienast et al., 2002), (4) Santa Barbara Basin and Point Conception (Emmer and Thunell, 2000; Hendy et al., 2004), (5) Guyamas Basin (Pride et al., 1999), (6) Mexico margin (Ganeshram and Pedersen, 1998), (7) Gulf of Tehuantepec (Thunell and Kepple, 2004; Hendy and Pedersen, 2006; Pichevin et al., 2010), (8) Nicaragua margin (Pichevin et al., 2010), (9) ODP1242 (Robinson et al., 2009; Martinez and Robinson, 2010), (10) Equatorial divergence Site ODP1240, same location as ME0005A-24JC (Robinson et al., 2009; Martinez and Robinson, 2010), (11) CD38-02 (Ganeshram et al., 2000), (12) GeoB7139-2, Chile margin (De Pol-Holz et al., 2006, 2007), (13) ODP1234 (Robinson et al., 2007), (14) ODP1233 (Martinez et al., 2006), (15) MD97-2120 (Pahnke and Zahn, 2005; Sachs and Anderson, 2005). (b) Oxygen concentration in the EEP at 200 m water depth (wd), derived from World Ocean Atlas 2005 (WOA05) (Garcia et al., 2006b). The OMZ of the ETNP and ETSP clearly appear in purple. The white dotted arrows show the Equatorial Undercurrent (EUC) splitting into northward and southward branches at the Galapagos Islands. The northward branch becomes the California Undercurrent (CU) while the southward branch joins the Peru–Chile Undercurrent (PCUC). (c) Map of the present-day mean annual SST distribution, derived from WOA05 (Locarnini et al., 2006). Black stars show locations of the studied cores. Black arrows indicate surface currents: North Equatorial Current (NEC), North Equatorial Counter Current (NECC), South Equatorial Current (SEC), Peru Current (PC). The equatorial Cold Tongue appears in green, with the Equatorial Front just to the north. Figure created using the software Ocean Data View (Schlitzer, 2010) (For interpretation of the references to colour in this figure legend, the reader is referred to the web version of this article).

atmospheric transport of water vapor, which leaves the Atlantic saltier than the Pacific.

Based on its key importance in Earth's present-day climate system, the tropical Pacific has been proposed as the trigger, amplifier, or mediator of past global climate change on time scales ranging from interannual to glacial–interglacial (e.g. Cane, 1998; Lea et al., 2000; Hostetler et al., 2006). Despite the efforts of many paleoceanographers, a mechanistic understanding of past changes of the eastern tropical Pacific and their linkages to high latitude remains missing or equivocal (Mix, 2006). Early studies addressed orbital-scale variations and the Last Glacial Maximum, with emphasis on changes in SST and productivity (e.g. Pedersen et al., 1991; Patrick and Thunell, 1997; Pisias and Mix, 1997; Mix et al., 1999; Feldberg and Mix, 2002, 2003; Loubere, 2002; Lyle et al., 2002; Lea et al., 2006).

More recent observations of millennial-scale variations in sea-surface salinity (SSS), SST, nutrient delivery, productivity and denitrification rates provide climate change signatures, independent of

longer-period orbital forcing, that link tropical climate fluctuations to variations in the high latitudes of the Northern or the Southern Hemisphere (e.g. Leduc et al., 2007; Kienast et al., 2006a; Robinson et al., 2007; Pena et al., 2008). Here we present new reconstructions of SST (based on alkenones), productivity (based on organic carbon and opal contents) and water-column denitrification (based on $\delta^{15}\text{N}$ of bulk organic matter) from four cores that span different hydrographic conditions across the Cold Tongue ($\sim 1^\circ\text{N}$ to $\sim 5^\circ\text{S}$) of the easternmost equatorial Pacific. We then use the data from the highest-resolution core (ME0005A-24JC) to examine mechanisms of millennial timescales oceanic variations in the EEP and linkages to higher-latitude climates.

2. Background

Millennial-scale climatic oscillations have occurred throughout the past few million years (Raymo et al., 1998). Synchronization of Greenland and Antarctic ice core records using the global

atmospheric change in CH₄ concentrations has revealed the existence of a bipolar seesaw (Blunier and Brook, 2001; EPICA, 2006). Rapid millennial (~1–2 ka period) oscillations in Greenland are referred to as Dansgaard–Oeschger (D–O) events; during a sequence of warm interstadial events in Greenland, Antarctica cools, whereas during cool stadials of the Northern Hemisphere, Antarctica warms. Although Northern Hemisphere events are asymmetric (rapid warming, slower cooling), the warm anomalies in Antarctica (called Antarctic Warm Events, AWE) are more symmetric. North Atlantic marine sediment cores reveal thick layers of ice-rafted debris, indicating that massive releases of icebergs (the so-called Heinrich Events, HE or H#) occurred during the coldest stadials in the Northern Hemisphere (see review in Hemming, 2004). D–O events appear to be associated with latitudinal shifts in oceanic convection between the Nordic Seas and the open mid-latitude Atlantic (Alley and Clark, 1999), whereas HE are associated with a significant slow down of NADW formation (McManus et al., 2004; Gherardi et al., 2005).

The triggers and hemispheric linkage mechanisms for millennial-scale changes are still debated. Two main hypotheses have been suggested as possible triggers: The first is a reorganization of the Atlantic meridional overturning circulation (e.g. Broecker et al., 1985), while the second one invokes changes in the dynamics of the tropical Pacific ocean–atmosphere system (Cane, 1998).

A key to sorting out these hypotheses is to determine the geographical extent of the climatic imprint associated with each hemisphere. For example, Rohling et al. (2009) showed that climate signals present in both Antarctica and Greenland ice core records influenced the Chinese speleothem $\delta^{18}\text{O}$ records (Fig. 1a – site 1), although the significance of their respective controls varies with time. Chronological correlations between these cave records and Greenland ice-core records were previously interpreted as reflecting a dominant control of Northern Hemisphere climate processes on monsoon intensity (Wang et al., 2001).

Given hypotheses on the role of the EEP in global climate mechanisms and a location where either hemisphere could influence the climatic record, it is important to assess the linkage of this region to the high latitudes of either or both hemispheres. Models have shown that the mid to high-latitudes can influence the tropical oceans via two pathways: the “atmospheric bridge” of the Hadley circulation and the “oceanic tunnel”, which involves subduction of Antarctic intermediate and mode waters in the sub-Antarctic region and their resurfacing in the equatorial Pacific after transit along the Equatorial Undercurrent (EUC, see Fig. 1a) (Liu and Yang, 2003).

Hydrologic variations in the eastern Pacific Warm Pool (EPWP), offshore central America, mimic the millennial-scale D–O oscillations that dominate Northern Hemisphere climate variability: higher paleosalinities coincide with Greenland stadials, a pattern explained by a southward migration of the Intertropical Convergence Zone (ITCZ) and/or a decrease in water vapor transport from the Atlantic to the Pacific Ocean (Fig. 1a) (Benway et al., 2006; Leduc et al., 2007).

North Atlantic derived climate forcing has also been invoked in alkenone-based SST reconstructions from the Panama Basin and the equatorial Cold Tongue region (Kienast et al., 2006a; Pahnke et al., 2007). These records show a significant cooling (~1.5 °C) during the time of North Atlantic Heinrich Event 1 (H1, ~16 kyr calendar BP). In this case, a more southerly ITCZ and strengthened northeasterly trade winds were invoked to explain the cooling in the Panama Basin, through enhanced coastal upwelling along the coast of Central America. Similarly, Koutavas and Sachs (2008) suggest that the deglacial temperature rise recorded by alkenone paleothermometry in the Cold Tongue follows a Northern Hemisphere tempo.

On the other hand, evidence from planktonic foraminiferal Mg/Ca thermometry in planktonic foraminifera suggests that tropical Pacific SSTs in both the Northern and Southern Hemispheres have covaried with Southern Hemisphere temperatures (Lea, 2004; Benway et al., 2006; Lea et al., 2006; Mix, 2006; Pena et al., 2008), and the Mg/Ca temperatures are in approximate agreement with those from species-based transfer functions (Feldberg and Mix, 2003). In this case, the connection between these two regions is envisioned as occurring either through direct response of each region to radiative (CO₂) forcing or through a physical link via oceanic circulation, through “the oceanic tunnel” or equatorward advection of waters in the Peru Current (Feldberg and Mix, 2003).

The oceanic tunnel has also been used to explain the biogeochemical and surface water productivity history of the EEP. Sarmiento et al. (2004) showed that Sub-Antarctic Mode Water (SAMW) has a strong influence on the nutrient content of the low-latitude thermocline. In the western equatorial Pacific, SAMW feeds into the EUC that then shoals eastward across the Pacific. Upwelling delivers EUC waters to the surface in the Cold Tongue region. A recent study focusing on the last glacial termination has shown that maxima in opal fluxes occur simultaneously in the EEP and south of the Antarctic Polar Front (APF) (Anderson et al., 2009). These authors suggest that enhanced upwelling of deep-water masses during the deglaciation caused an increased supply of silicic acid to surface waters south of the APF. Some of this silicic acid was subsequently entrained in the thermocline and advected towards low-latitude regions.

This hypothesis supports the scenario proposed by Spero and Lea (2002), suggesting that the deglacial minimum in $\delta^{13}\text{C}$ of planktonic foraminifera observed in low-latitude records reflects a higher nutrient content and corresponds to a chemical signature of increased upwelling of deep water in the Southern Ocean. Indeed, there is strong evidence in the EEP for enhanced nutrient content of subsurface EUC waters during this interval. The highest rate of organic carbon accumulation during the last 35 kyr occurs during this time window (Kienast et al., 2006a) and residual sedimentary $\delta^{15}\text{N}$ records (Fig. 1a – site 10), corrected for regional denitrification, show a coeval decrease in the degree of surface-water nitrate consumption (Robinson et al., 2009). Thus, during the deglaciation, the supply of nutrients exceeded the apparently high demand implied by the organic carbon flux maximum identified by Kienast et al. (2006a). Martinez and Robinson (2010) propose that the increase in export production during the deglaciation resulted in higher subsurface oxygen demand, which led to an intensification of water column denitrification within the OMZs of the SE and NE Pacific margin (Fig. 1a – sites 9 and 10).

On a longer time-scale, sedimentary $\delta^{15}\text{N}$ records from the southern margin of the eastern tropical South Pacific (ETSP) OMZ appear to be responding to Southern Hemisphere climate changes (Fig. 1a – sites 12–14): peaks in denitrification are in-phase with AWE (De Pol-Holz et al., 2007; Robinson et al., 2007). Robinson et al. (2007) explain the timing as originating from bio-physical changes in the region of SAMW formation. SAMW feeds into the EUC, which then flows into the Peru–Chile Undercurrent to become the primary source of the upwelled water along the Peru margin that fuels the high export of organic matter and consequently the suboxia in the subsurface (Toggweiler et al., 1991; Spero and Lea, 2002; Sarmiento et al., 2004). Alternatively, the $\delta^{15}\text{N}$ variations in the ETSP could reflect local hydrographic changes, such as dilution of isotopically heavy nitrate in the Peru–Chile Undercurrent by lighter southern sourced water (Martinez et al., 2006), collapse of the thermocline ventilation caused by fresh-water pulses from the Patagonian Ice Sheet (De Pol-Holz et al., 2006) or retreat of stronger, more oxygenated glacial Antarctic Intermediate Water synchronously with Antarctic warming and southward translation of the southern westerlies (Muratli et al., 2010).

Table 1
Core locations and water depth.

Core	Latitude	Longitude	Water depth
ME0005A-24JC	0°01.30'N	86°27.79'W	2941 m
ME0005A-27JC	1°51.20'S	82°47.20'W	2203 m
TR163-31P	3°37.12'S	83°58.24'W	3205 m
TR163-19P	2°15.50'N	90°57.10'W	2348 m

Pichevin et al. (2010) suggest that this Southern Hemisphere timing affects $\delta^{15}\text{N}$ records from the Nicaragua Basin ($\sim 12^\circ\text{N}$) and is still noticeable in the Gulf of Tehuantepec ($\sim 15^\circ\text{N}$) (Fig. 1a – sites 7 and 8). These authors imply leakage of heavy nitrate sourced in the ETSP across the equator. Previous studies on the other hand suggest that the hemispherically synchronous changes in denitrification result from the EUC feeding both the northward and southward flowing poleward undercurrents (Fig. 1b) (Tsuchiya and Talley, 1998; Kienast et al., 2002; Robinson et al., 2009).

Studies from further north along the NE American margin detected North Atlantic derived climate forcing in their downcore sedimentary $\delta^{15}\text{N}$ record (Fig. 1a – sites 3–5) (Pride et al., 1999; Emmer and Thunell, 2000; Hendy et al., 2004). Along the Californian margin and further north, these oscillations were initially interpreted as reflecting changes in denitrification in the eastern tropical North Pacific (ETNP) OMZ (Emmer and Thunell, 2000; Kienast et al., 2002). However, later studies of sedimentary $\delta^{15}\text{N}$ from the core of the ETNP OMZ did not find a clear North Atlantic derived climate forcing (Thunell and Kepple, 2004; Hendy and Pedersen, 2006). Thus the North Atlantic derived climate forcing evident further north was reinterpreted as either reflecting variations in the rate of upwelling of deeper water masses enriched in heavy $\delta^{15}\text{N}$ travelling northward along the coast or as reflecting ventilation variations by North Pacific Intermediate Water (Hendy and Pedersen, 2006).

In summary, it remains unclear whether on a millennial time-scale the EEP responded primarily to a Southern or Northern Hemisphere forcing. Here, we use alkenone SST, denitrification and productivity proxies to identify the climate forcings that resulted in the hydrographic changes recorded in the Eastern Tropical Pacific over the last climatic cycle, with a focus on MIS 2–4. We evaluate two mechanisms suggested to control oceanic variability in the EEP: an atmospheric bridge scenario forced by Heinrich Events that results in an enhancement of NE trade winds, a southward movement of the ITCZ and Westerlies, and an intensification of intermediate water circulation. The second mechanism is an oceanic tunnel one, whereby warming of Southern Ocean surface waters during AWE reduces the oxygen content of intermediate waters, expanding the ETNP and ETSP denitrification zone and warming subsurface water upwelled in the EEP.

3. Material and methods

3.1. Core material and study site

We present new records of alkenone based SST, bulk sediment nitrogen isotopic composition, opal concentration and organic carbon content of 4 cores from the EEP covering the last 100 kyr. Sediment cores ME0005A-24JC and ME0005A-27JC were recovered during the ME0005A expedition aboard the *R/V Melville* in 2000. Sediment cores TR163-19P, and TR163-31P were recovered during the cruise 163 aboard the *R/V Trident* in 1975. Core locations are shown in Fig. 1a and c and listed in Table 1.

The sites are strategically located across this complex oceanographic region to detect hydrographic and biogeochemical changes and evaluate the importance of the northern and southern polar

influences (Fig. 1). Two distinct upwelling systems co-exist in the EEP. The first is located off Peru, where upwelling taps deep sub-Antarctic-sourced, nutrient-rich water. This stimulates intensive production in the Cold Tongue as it recirculates into the south equatorial current (Toggweiler et al., 1991; Toggweiler and Carson, 1995; Dugdale et al., 2002). Core sites TR163-31P and ME0005A-27JC are affected most by these highly productive waters. The second system is farther from the coast where the source of upwelling is relatively shallower waters brought up via the equatorial divergence (Dugdale et al., 2004). Core ME0005A-24JC is situated within this equatorial divergence zone. Core TR163-19P is located in warmer waters lying north of the Equatorial Front for most of the year. Thus the cores span a gradient in biological productivity with higher values ($200\text{ gC/m}^2/\text{yr}$) observed at sites TR163-31P and ME0005A-27JC close to the Peru upwelling and lower values ($140\text{ gC/m}^2/\text{yr}$) at site TR163-19P at the northern limit of the shallow equatorial upwelling zone (Antoine et al., 1996).

3.2. Analytical methods

Cores ME0005A-24JC, ME0005A-27JC and TR163-31P were analyzed for alkenone unsaturation at Dalhousie University. Total lipids were extracted from 1.5 to 3 g aliquots of freeze-dried sediment samples using a Dionex Accelerated Solvent Extraction system (ASE200). These extracts were saponified using potassium hydroxide and purified through silica column chromatography. The purified extracts were analyzed by gas chromatography (Agilent 6890N) at Dalhousie. Sea-surface temperature estimates (UK'37 SST) were calculated from the ratio of the concentration of the di- and triunsaturated alkenones, using the calibration of Prahl et al. (1988). The upper 500 cm of ME0005A-24JC were analyzed at WHOI following the same procedure and were previously published by Kienast et al. (2006a). These data were shifted by $+0.027$ UK'37 units because of a laboratory offset determined from 10 replicate samples. Cores TR163-19P was analyzed at Brown University following similar laboratory procedures detailed in Herbert et al. (1998). Results from the last 25 kyr BP of cores ME0005A-27JC, TR163-19P and TR163-31P were previously published in Dubois et al. (2009).

The sedimentary $\delta^{15}\text{N}$ composition of all cores was analyzed at the Pacific Centre for Isotopic and Geochemical Research, UBC Vancouver. Samples were freeze dried, ground in an agate mortar, packed in tin cups and measured by combustion using a Carlo Erba NC 2500 elemental analyzer coupled to a Finnigan Mat Delta Plus mass spectrometer, via a Finnigan Mat ConFlo III inlet. Normalization to the international $\delta^{15}\text{N}_{\text{air}}$ scale was done by running four repeats of an internal laboratory standard (Acetanilide [4.0]) and one international isotope reference material (IAEA-N1 [0.4] or IAEA-N2 [20.3]) with every batch of 24 samples. Reproducibility for $\delta^{15}\text{N}$ was better than $\pm 0.2\%$.

Total carbon was determined by flash-combustion gas chromatography with an elemental analyzer using operational conditions similar to those described by Verardo et al. (1990). Relative standard deviation (R.S.D.) was $\pm 2\%$ of measured values (1σ) based on two internal sedimentary standards analyzed along with the samples. Inorganic (i.e., carbonate mineral) carbon was determined by CO_2 evolution after HCl treatment of weighed bulk sediment samples in a carbon dioxide coulometer with an analytical precision of $\pm 2.3\%$ (1σ , R.S.D.). Organic carbon was estimated by subtracting inorganic from total carbon, with a combined analytical precision (as R.S.D.) of $\pm 3\%$. Results for the last 35 kyr have been published by Kienast et al. (2006a, 2007).

Biogenic opal (Si_{opal}) of core ME0005A-24JC (>510 cm) was determined at Dalhousie University by extraction of silica from 20 mg subsamples by a 2 M Na_2CO_3 solution at 85°C for 5 h.

Table 2
Radiocarbon Data of Core ME0005A-24JC.

	Core depth [cmbsf]	¹⁴ C age [yr]	Calendar age ^a [yr BP]	Reference
<i>N. dutertrei</i>	15–20	3255 ± 30	2870 ± 130	Kusch et al. (2010)
<i>N. dutertrei</i>	46–51	7100 ± 40	7450 ± 100	Kusch et al. (2010)
<i>N. dutertrei</i>	81	9040 ± 40	9550 ± 130	Kienast et al. (2007)
<i>N. dutertrei</i>	230	13,900 ± 35	16,410 ± 320	Kienast et al. (2007)
<i>N. dutertrei</i>	291	15,700 ± 85	18,200 ± 120	Kienast et al. (2007)
<i>N. dutertrei</i>	351	18,050 ± 65	20,790 ± 280	Kienast et al. (2007)

^a Calibrated to calendar ages with the software CALIB 6.0 (Stuiver and Reimer, 1993) using a reservoir correction of $\Delta R = 167 \pm 106$ yr and the calibration data set Marine09 (Reimer et al., 2009). Calendar ages are rounded to the nearest 10 yr.

Dissolved silica concentrations in the extract were determined by molybdenum blue spectrophotometry (Mortlock and Froehlich, 1989). The upper 510 cm were analyzed at UBC following the same procedure and were previously published by Kienast et al. (2007). Percent opal is calculated as $2.4 \times Si_{opal}$. The relative standard error from duplicates was $\pm 2.1\%$.

3.3. Age models

Age models for Marine Isotopic Stage 1 and 2 (MIS1 and MIS2, i.e. 0–25 kyr) in cores ME0005A-27JC, TR163-19P and TR163-31P were adopted as previously published (see Kienast et al., 2007). We present here an updated MIS1–2 age model of core ME0005A-24JC based on 4 radiocarbon dates on *Neogloboquadrina dutertrei* published by Kienast et al. (2007) and 2 additional dates on *N. dutertrei* published by Kusch et al. (2010) (Table 2). Radiocarbon ages were calibrated to calendar years using the software CALIB 6.0 (Stuiver and Reimer, 1993; $\Delta R = 167 \pm 106$ yr), and the MARINE09 calibration data set (Reimer et al., 2009). Note that the use of this new calibration data set (MARINE09) leads to small deviations (<600 yr) from the calendar ages published by Kienast et al. (2007) using the MARINE04 (Hughen et al., 2004) calibration data set.

Because of the difficulty in dating sediments from the equatorial Pacific older than 50,000 yr (see discussion below), we created two different age models based on the hypotheses under investigation. In this approach, we correlate millennial-scale events observed during MIS3 in the opal (scenario 1) and in the $\delta^{15}N$ records (scenario 2) of ME0005A-24JC to the new high-resolution $\delta^{18}O_{ice}$ EPICA Dronning Maud Land (EDML) record from Antarctica. The $\delta^{18}O_{ice}$ EDML record is synchronized in detail to the GICC05-based

Table 3
Correlation points used between ME0005A-24JC and EDML1.

Depth in ME-24 [cmbsf]	Age [kyr BP]	Tie point
<i>Scenario 1^a</i>		
550	36.25	
592.5	38.9	AWE1
603	39.6	
671.5	46.5	AWE2
720	54.4	AWE3
770.5	58.8	AWE4
800	61.3	
<i>Scenario 2^b</i>		
504	38.90	AWE1
660	46.50	AWE2
752	54.40	AWE3
804	58.80	AWE4
840	66.25	
900	71.17	AWE5
932	74.5	AWE6
968	80.71	

^a MIS3 opal maxima (filtered) were matched with EDML $\delta^{18}O_{ice}$

^b MIS3 $\delta^{15}N$ maxima were matched with EDML $\delta^{18}O_{ice}$

Greenland $\delta^{18}O_{ice}$ records via methane concentration in air bubbles trapped within the ice (EPICA Community Members, 2006). The MIS3 tie points are presented in Table 3. We then examine the repercussions that this matching has on the other proxies and mechanisms implied.

Cores TR163-31P, TR163-19P and ME0005A-27JC were graphically correlated to ME0005A-24JC for the MIS3–4 interval using the software AnalySeries (Paillard et al., 1996). We based our correlation on a number of clear features in the $\delta^{15}N$ and opal records, making sure not to violate the MIS4 benthic $\delta^{18}O$ transitions. We thus make the explicit assumption that events evident in the proxy record of all the cores occur synchronously across the EEP. Finally, based on multiple geochemical proxies (not shown), we identify an ash layer at a depth of 9.8 m in ME0005A-24JC, 4.31 m in ME0005A-27JC, 3.10 m in TR163-19P and 6.61 m in TR163-31P, which we assume to be the Los Chocoyos Ash Layer. This Ash Layer was previously observed in the Gulf of Mexico and equatorial Pacific and has been dated to 84,000 yr BP on the basis of oxygen isotope stratigraphy, biostratigraphy and Pa–Th data (Drexler et al., 1980). The absolute accuracy of the individual age models is not crucial in the context of this study, since our primary conclusions are based on the phase relationship among different proxies within the same core (ME0005A-24JC). The additional cores serve only as controls as to whether the features we observe are representative of a regional signal.

We rely on tuning for the MIS3 intervals for three main reasons. First, radiocarbon dating can only be used for the last 50,000 kyr, and with increasing uncertainties (Faibanks et al., 2005). Second, the absence of clearly defined benthic $\delta^{18}O$ events or transitions during MIS3 would not allow tight age control. In addition, it has been recently shown that $\delta^{18}O$ transitions are not synchronous between ocean basins (Skinner and Shackleton, 2005; Lisiecki and Raymo, 2009). And third, precisely dated geomagnetic excursions such as the Laschamp Event (~41 kyr BP; Singer et al., 2009) could not be detected at our core locations close to the equator. We draw the reader's attention to the fact that this tuning approach will not become circular. We only use it to test what the implications of a particular scenario are.

4. Results and interpretation of local processes

4.1. SST

The UK'37-SST profile of core ME0005A-24JC shows a long-term decreasing trend from 100 to 17 kyr BP, followed by a more rapid continuous warming during the deglaciation and the Holocene (Fig. 2a). The highest SSTs are reached during MIS5 (~27 °C) and the Holocene (26.7 °C). Although the LGM (19–23 kyr BP) is colder than the Holocene, the absolute minimum of SST during the last 100 kyr is observed around 16 kyr BP during the deglaciation (Kienast et al., 2006a). Warm excursions of up to 1.5 °C occurred as relatively short events (>5 kyr) during MIS3.

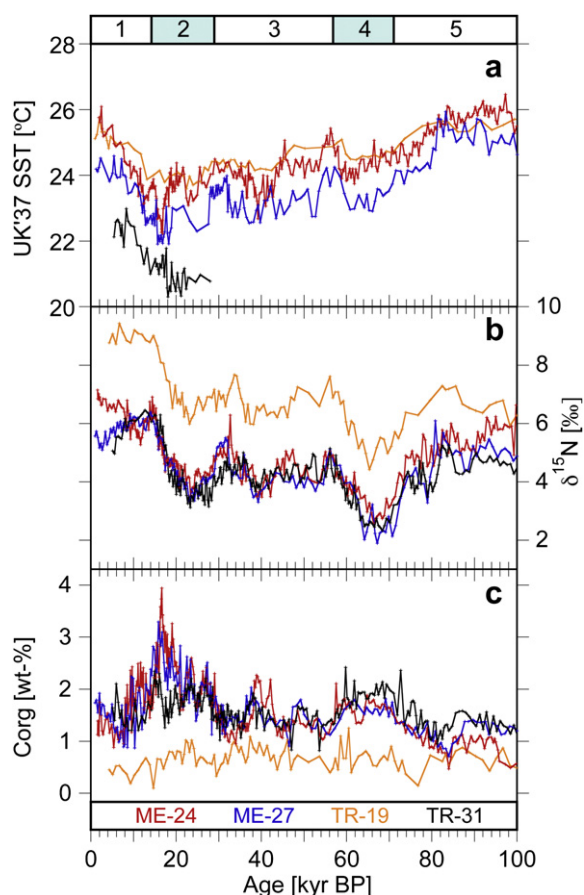


Fig. 2. Downcore records of sea surface temperature (a), bulk sediment nitrogen isotope ratios (b) and organic carbon content (c) in the four cores for the last 100 kyr. Cores are distinguished by different colors (see legend). The records are plotted following the age model of scenario 1 (see text). Blue and white rectangles at the top indicate the Marine Isotopic Stages 1–5 (For interpretation of the references to colour in this figure legend, the reader is referred to the web version of this article).

The UK'37-SST profiles of core ME0005A-27JC and TR163-19P show very similar features, in particular the long term decreasing trend up to the deglaciation superimposed by a number of millennial-scale warmings (Fig. 2a). These warmings are of smaller amplitude in TR163-19P, but this might be due to the lower sedimentation rates and resolution of this core (average sampling resolution for alkenone SST determination is 340 yr in ME0005A-24JC, 830 yr in ME0005A-27JC and 1370 yr in TR163-19P). The UK'37-SST profile of core TR163-31P is too short to make any conclusive interpretation. The SST difference between ME0005A-24JC and ME0005A-27JC remains relatively constant over the last 100 kyr, except during rapid and pronounced cooling intervals in ME0005A-24JC during which the SST gradient is minimal.

Advection of colder water in the EUC and its subsequent upwelling would be expected to affect the two upwelling centers (equatorial and marginal) similarly and thus should not lead to a smaller gradient between ME0005A-24JC and ME0005A-27JC. Because the millennial-scale coolings are also recorded in core ME0005A-43JC (7°51.35'N, 83°36.50'W) in the EPWP (Dubois et al., in preparation), stronger advection of the Peru Current as suggested for the Last Glacial Maximum (e.g. Feldberg and Mix, 2002; Dubois et al., 2009) appears to be unlikely, as would be a westward extension of the Peru upwelling system. A decrease in the SST gradient between ME0005A-24JC and ME0005A-27JC during the short cooling intervals thus most likely reflects either a wind pattern that would enhance equatorial upwelling relative to the

Peru upwelling, or advection of colder water upwelled further north in the Panama Basin to site ME0005A-24JC. The latter has been suggested in a modeling study by Zhang and Delworth (2005) that simulated cooling north of the equator in response to a substantial weakening of the Atlantic thermohaline circulation imposed by freshwater forcing.

4.2. Organic carbon

The organic carbon concentration in ME0005A-24JC varies between 0.5 and 4 wt% during the last 100 kyr (Fig. 2c, average sampling resolution for %C_{org} measurements is 330 yr in ME0005A-24JC, 390 yr in TR163-31P, 540 yr in ME0005A-27JC and 880 yr in TR163-19P). The highest amplitude peak occurs during the deglaciation (14–20 kyr BP), as described in Kienast et al. (2006a) and Martinez and Robinson (2010). This peak is superimposed on values already somewhat higher from 7 to ~30 kyr BP. Additional intervals of slightly higher values occur between ~35 and 45 kyr BP and between ~55 and 70 kyr BP. Similar oscillations can be observed in ME0005A-27JC and TR163-31P, which record a more pronounced positive excursion from ~45 to ~50 kyr BP (Fig. 2c). On the other hand, TR163-19P records lower organic carbon content (0–1 wt%). This pattern is predictable given that TR163-19P is located at the northern limit of the equatorial upwelling. In all these cores, Th-normalized fluxes (not shown) generally agree well with the organic carbon concentration (see also Kienast et al., 2006a, 2007; Pichevin et al., 2009), supporting our interpretation of organic carbon concentration changes as representing carbon flux changes.

The similarity of these organic carbon records between the 3 core sites in the EEP indicates that they reflect regional fluctuations. Recall that ME0005A-24JC is situated within the equatorial divergence zone, while TR163-31P and ME0005A-27JC are affected most by the highly productive waters from the Peru upwelling. Therefore the overall good covariation among these records indicates that they are not influenced by local processes at the deposition site, but rather by regional changes in nutrient delivery and productivity.

During MIS2–4, the millennial-scale intervals of higher organic carbon content are mirrored by intervals of lower $\delta^{15}\text{N}$ (Fig. 2b). Cross-spectral analysis reveals that organic carbon and $\delta^{15}\text{N}$ variations are significantly anti-correlated on timescales longer than 2500 yr, with a peak at 5000 yr. Therefore, the export fluxes in the EEP upwelling systems and the associated drawdown in subsurface oxygen concentration cannot be implied as the cause of changing downstream denitrification rates as suggested for the deglaciation (Martinez and Robinson, 2010).

4.3. $\delta^{15}\text{N}$

The average bulk sedimentary $\delta^{15}\text{N}$ of core ME0005A-24JC over the last 100 kyr is 5‰ (Fig. 2b). MIS5 shows a slowly decreasing trend, from 6 to 5‰. MIS4 on the other hand shows the lowest values (2.6‰) of the record. During MIS3, a series of 1–2‰ variations occur on a timescale of 5–10 kyr (the same sampling resolution was used as for %C_{org} measurements). $\delta^{15}\text{N}$ values increase steadily since the LGM from 3.5 to 7.1‰ in the top-most sample, with the exception of a positive excursion during the Bölling–Allerød period. Cross-spectral analysis reveals that $\delta^{15}\text{N}$ and SST variations are significantly coherent at timescales longer than ~3000 yr. On a millennial-scale, the warm excursions generally coincide with high $\delta^{15}\text{N}$ values.

The increase in $\delta^{15}\text{N}$ during the Bölling–Allerød is seen in all of the records from the ETNP and the Arabian Sea and represents one of the most significant changes in the marine nitrogen cycle during the last 25 kyr (Thunell and Kepple, 2004). The pronounced

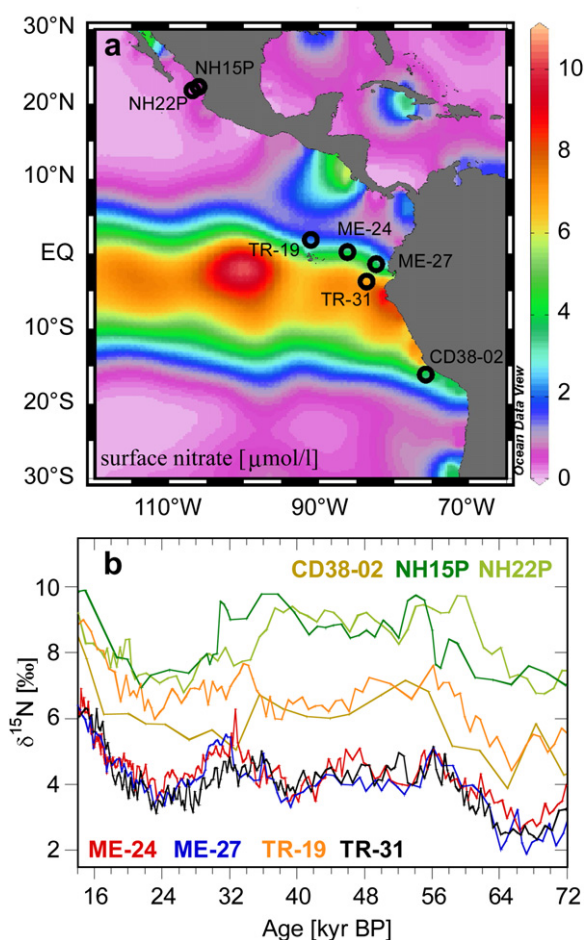


Fig. 3. (a) Core locations on a map of mean annual nitrate concentrations in surface waters. Figure created using the software Ocean Data View (Schlitzer, 2010) and data from WOA05 (Garcia et al., 2006a). (b) Bulk sediment nitrogen isotopic record during MIS2–4 from our four EEP cores (see legend at the bottom). Shown for comparison are cores NH15P and NH22P from the Mexico Margin (Ganeshram and Pedersen, 1998) and core CD38-02 from the Peru Margin (Ganeshram et al., 2000) (see legend at the top). Note that the offset between the records from the EEP and the Mexico and Peru margins is most likely due to uncertainties in the age control of the latter records.

minimum occurring during MIS4 is also common to a number of $\delta^{15}\text{N}$ records from other oceanic regions (e.g. Galbraith et al., 2004).

Sedimentary $\delta^{15}\text{N}$ records represent a complex amalgam of local and more distal processes. Downcore $\delta^{15}\text{N}$ records are potentially influenced by many factors including the input of land-derived organic material, changes in the isotopic offset due to alteration during sinking or sedimentation, local changes in denitrification rates, changes in the degree of nitrate consumption, and changes in the source of nitrate and/or its isotopic composition.

Input of land derived organic material is unlikely to play a dominant role because it would have had a stronger influence in ME0005A-27JC, the core closest to coast, which is not supported by the similarity of values in this core and the other cold-tongue cores. Similarly, local water-column denitrification at our core sites is unlikely due to the influence of the oxygen-rich EUC (Fig. 1b). As for the diagenetic imprint, previous studies have shown little temporal variations of this effect on $\delta^{15}\text{N}$ in sediments from the Equatorial Pacific (e.g. Altabet and Francois, 1994). Thus we are left with two potential mechanisms controlling the $\delta^{15}\text{N}$ signal recorded in the EEP: (1) changes in the degree of nitrate consumption and (2) changes in the isotopic composition of the source of nitrate.

Although cores TR163-31P, ME0005A-24JC and ME0005A-27JC are located in different oceanic regimes (see Section 3.1), spanning

500 km overall (Fig. 1), their sedimentary $\delta^{15}\text{N}$ records show a very close correspondence during the last glacial stage, as do their C_{org} records (MIS2–4, Fig. 2b). TR163-19P, which is located further away from the equatorial divergence records higher $\delta^{15}\text{N}$ values reflecting the increased nutrient utilization as the surface water is advected away from the equator (Fig. 2b) (c.f. Farrell et al., 1995; Robinson et al., 2009). The offset between $\delta^{15}\text{N}$ at TR163-19P and the three cores further south has remained constant during MIS2–4. However, the interglacials MIS1 and MIS5 clearly show a different pattern with diverging $\delta^{15}\text{N}$ gradients between our 4 locations, reflecting local changes in nutrient utilization during the warmer stages (Dubois et al., in preparation). At present, these four cores are located on a gradient of surface nitrate concentration (Fig. 3a, from 2 to 7 $\mu\text{mol/l}$) as well as a gradient in surface sediment $\delta^{15}\text{N}$ (see Fig. 2a in Farrell et al., 1995, from 5 to 9‰). Thus the close convergence of the three southern records during the last glacial stage is quite remarkable. We interpret the highly coherent variations during MIS2–4 as evidence for the absence of significant local changes in nutrient utilization over this time period.

However, the perfect similarity between the three $\delta^{15}\text{N}$ records, both in terms of variations and absolute values, could reflect large-scale regional changes in the ratio between the biological uptake and the nitrate supply. As shown by the C_{org} content records (Fig. 2c), similar variations in biological uptake/production occurred at the 3 southern sites during MIS2–4. The millennial-scale intervals of higher organic carbon content are mirrored by intervals of lower $\delta^{15}\text{N}$ (Fig. 2b), which would – in this case – indicate a decrease in relative nitrate utilization. In the Equatorial Pacific, uptake of nitrate is ultimately controlled by the availability of iron (Martin et al., 1991; Chai et al., 1996; Fitzwater et al., 1996). Thus changes in the degree of nitrate consumption require that the surface waters witness variations in the iron-to-nitrate ratio ($\text{Fe}:\text{NO}_3^-$) and not just the net supply of nutrients (Robinson et al., 2009). To create such a pattern of high uptake-low utilization would require an increased supply of both Fe and NO_3^- (to increase biological production), but with a lower $\text{Fe}:\text{NO}_3^-$ ratio (to lower relative nitrate utilization).

We dismiss regional changes in nitrate utilization as a primary control on the EEP downcore $\delta^{15}\text{N}$ data for two main reasons. First, if temporal changes in relative utilization were a dominant factor in EEP sedimentary $\delta^{15}\text{N}$ records, we would expect a significant increase in relative utilization (higher $\delta^{15}\text{N}$) during the dustier glacial interval, due to eolian Fe fertilization (assuming nitrate supply was relatively constant), which is not observed. Second, the relationship between $[\text{NO}_3^-]$ and $\delta^{15}\text{N}$ in the EEP is exponential, due to Rayleigh fractionation. Thus, regional changes in the ratio of supply to demand would impact the spatial $\delta^{15}\text{N}$ gradients in a non-linear way, which is also not observed. In conclusion, we make the assumption that the balance between supply and demand is maintained during MIS 2–4 by a constant $\text{Fe}:\text{NO}_3^-$ ratio in upwelling waters. A similar observation was made for present-day condition by Altabet (2001) during the US JGOFS EqPac program. Despite a doubling of surface $[\text{NO}_3^-]$ accompanying relaxation of El Niño conditions, relative utilization of NO_3^- remained nearly constant.

Thus, based on the similarity of our records, we assume that the millennial-scale $\delta^{15}\text{N}$ oscillations recorded during MIS2–4 reflect temporal variations in the isotopic signature of the regional nitrogen pool. The question then becomes what processes drive changes in this regional nitrate pool? The isotopic composition of the nitrate upwelled in the EEP is determined by the isotopic composition of the primary source of nitrate (SAMW) and by denitrification in the adjacent OMZs. Although we cannot exclude influences of isotopic variations in SAMW, two lines of evidence support our assumption that the MIS3 oscillations reflect changes

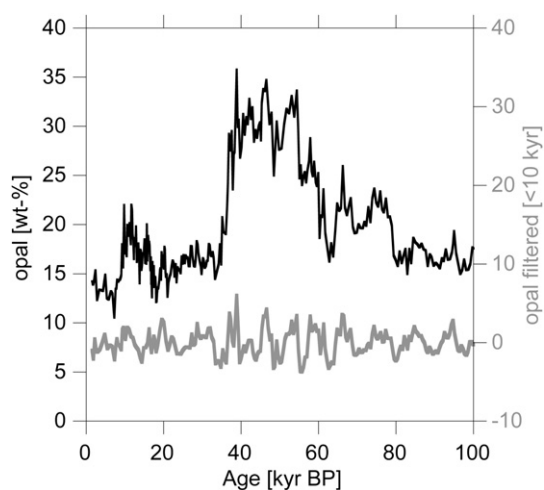


Fig. 4. Opal record of ME0005A-24JC for the last 100 kyr. In black, the opal content. In grey, the residual opal record, once variability >10 kyr is removed from the black record (see text).

in denitrification intensity in the Eastern Pacific. First, on orbital timescales Robinson et al. (2009) have shown that changes in the $\delta^{15}\text{N}$ of preformed nitrate in the EUC (approximated by diatom $\delta^{15}\text{N}$ records from the Southern Ocean) are of opposite sign to the EEP $\delta^{15}\text{N}$ variations. Second, the pattern of change in our new EEP $\delta^{15}\text{N}$ records is quite similar to the variations in $\delta^{15}\text{N}$ recorded in the sediments underlying and downstream from the large regions of water column denitrification in the ETP (Ganeshram et al., 2000; Kienast et al., 2002; Hendy et al., 2004; De Pol-Holz et al., 2007; Robinson et al., 2007). Fig. 3b shows a comparison to denitrification records from the Mexico Margin (cores NH15P and NH22P) (Ganeshram and Pedersen, 1998) and from the Peru Margin (core CD38-02) (Ganeshram et al., 2000). Note that the age models of these cores are based on low-resolution oxygen isotope stratigraphy. Sedimentary $\delta^{15}\text{N}$ records from these cores have been suggested to represent pure water column denitrification signals since no net isotopic fractionation occurs when nitrate is completely consumed annually in the surface waters, as occurs at these locations, in particular on the Mexico Margin (Fig. 3a). The coherent variations over such a large geographic extent strongly support the assumption that the EEP records reflect an advected denitrification signal as opposed to changes in nitrate utilization.

Previous studies suggest an active exchange between the subsurface nitrate underlying the EEP and the denitrified water offshore Peru (Toggweiler and Carson, 1995). Indeed, Robinson et al. (2009) estimate that at least 30% of the nitrate pool underlying the EEP comes from exchange with or advection from the ETSP OMZ. We follow this reasoning and assume that the denitrification signal recorded in our cores originates in the ETSP OMZ.

4.4. Percent biogenic opal

Percent opal is often used as an indicator of diatom productivity (e.g. Charles et al., 1991). In ME0005A-24JC, as in other EEP records, a large peak characterizes opal concentration during MIS3, which precludes interpreting millennial-scale variations (see Kienast et al., 2006b). Dubois et al. (in press) interpret this peak as a preservation event, reflecting possibly heavier silicification of the diatoms due to Fe limitation. The “background” opal concentration is around 15 wt%, while during the MIS3 peak opal concentrations reach 35 wt%. Assuming that the preservation event is a long-term event superimposed on shorter-term variations in opal productivity, we use

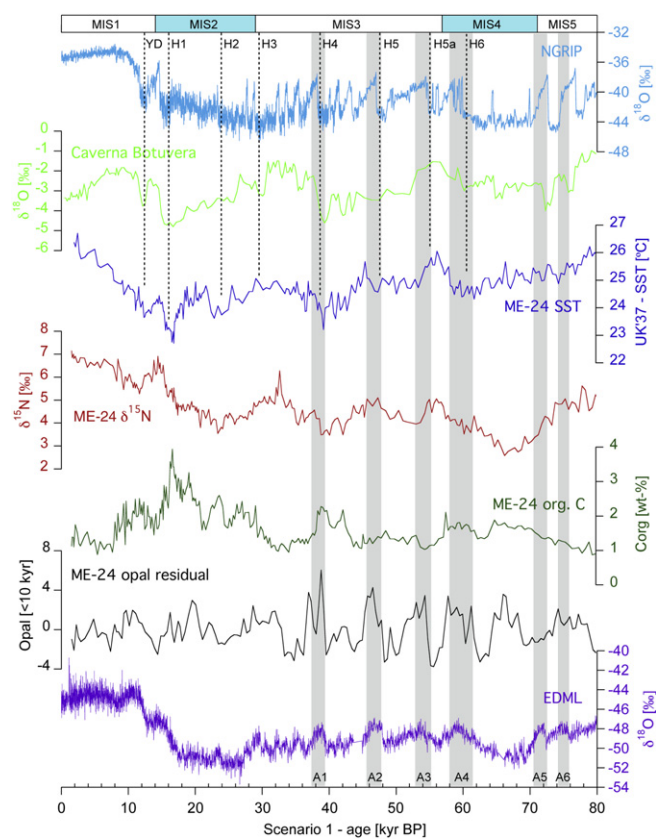


Fig. 5. Multi proxy record of SST, $\delta^{15}\text{N}$, organic carbon and residual opal from core ME0005A-24JC, plotted on the age scale obtained with scenario 1 (see Section 5.1 in the text). Shown for comparison are the $\delta^{18}\text{O}$ records from NGRIP (light blue, Greenland ice core), Caverna Botuvera (light green, South Brazil speleothem), EDML (purple, Antarctica ice core). Shaded areas represent Antarctic Warm Events (A1–A6). Dotted lines indicate the Younger Dryas (YD) and the Heinrich Events (H1–H6). The Marine Isotopic Stages (MIS) are indicated by the blue and white rectangles at the top (For interpretation of the references to colour in this figure legend, the reader is referred to the web version of this article).

a high-pass band filter to remove variability >10 kyr BP (Fig. 4). This gives rise to a set of clearly defined millennial-scale oscillations during MIS3 of a maximum amplitude of 10 wt%.

5. Discussion

5.1. Scenario 1 – chronology and implications

In scenario 1, we follow Anderson et al.'s (2009) scenario to constrain the age model during MIS3. We match the millennial-scale peaks in the filtered opal record with the AWE observed in the EDML $\delta^{18}\text{O}_{\text{ice}}$ record (Table 3). As shown in Section 2, this hypothesis, i.e. changes in the nutrient content of SAMW affecting the EEP, was initially proposed for the deglaciation only. However, Anderson et al. (2009) clearly observe similar peaks in opal flux in the Southern Ocean during MIS3, which they attribute to increased upwelling of deep water south of the polar front and subsequent advection to the Sub-Antarctic during each AWE. It is thus legitimate to look for a signal transmitted to the EEP during MIS3, similar to what occurs during the deglaciation.

Fig. 5 presents the multiple proxy records of ME0005A-24JC plotted on this age-scale. With this age model, the alkenone SST reconstruction indicates colder intervals coeval with the Northern Hemisphere HE, with the exception of H5a. Scenario 1 is thus consistent with the hypothesis of a North Atlantic derived climate

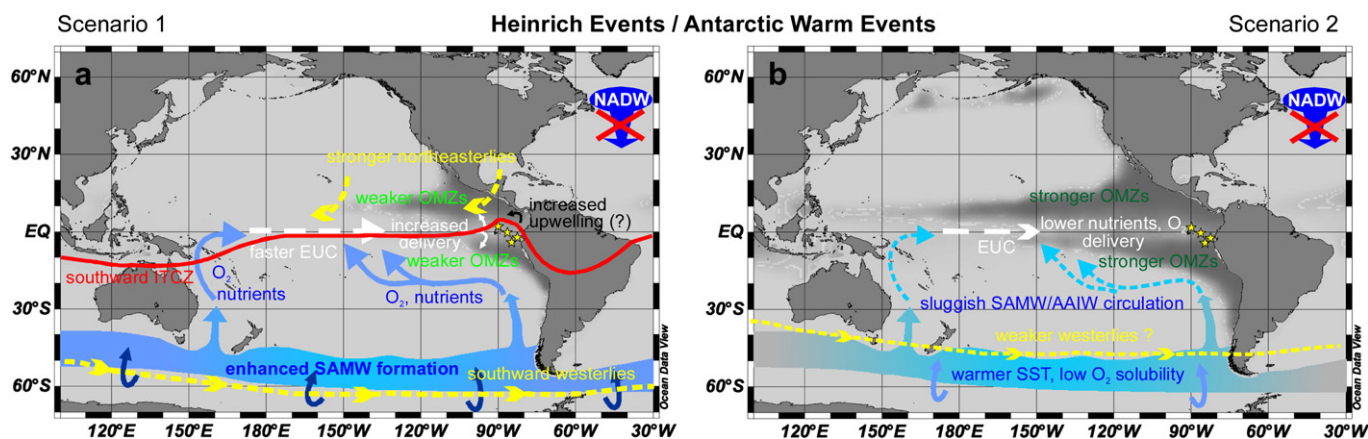


Fig. 6. Schematic illustration of the various processes occurring during the Heinrich Events/Antarctic Warm Events in scenario 1 (a) and scenario 2 (b). (a) During the Heinrich Events, NADW formation turns off. This results in a southward shift of the ITCZ and the southern hemisphere westerlies. The new poleward position of the westerlies enhances upwelling of deep water around Antarctica and – in scenario 1 – the formation rate of SAMW. The stronger easterlies increase the thermocline tilt along the equator, increasing the speed of the EUC. Enhanced thermocline circulation in this scenario increases the delivery of nutrients and O₂ to the Eastern Pacific. The rapidly flushed thermocline lessens the spatial extent of the OMZ and/or denitrification intensity. (b) In scenario 2, sluggish Southern Ocean circulation of warmer, less oxygen-rich thermocline waters causes expansion of denitrification zones during the Antarctic Warm Events.

forcing of SST changes in the equatorial Cold Tongue, as suggested by Kienast et al. (2006a), Pahnke et al. (2007) and Koutavas and Sachs (2008). H1 and H4 stand out as the most pronounced cooling intervals (see also Section 4.1), during which the SST in ME0005A–24JC reaches the cooler SST recorded in ME0005A–27JC. The lower resolution of ME0005A–27JC may prevent us from detecting the same pattern during the other HE.

As observed during H1 (Kienast et al., 2006a), the organic carbon record on this age scale suggests increases during earlier Heinrich Events, with the exception of H5. During H1 and H4, the two most pronounced cooling intervals, the organic carbon content in ME0005A–24JC exceeds that in ME0005A–27JC (Fig. 2c).

As stated in Section 4.2, millennial-scale variations in the $\delta^{15}\text{N}$ record seem to covary with the SST records, in particular during MIS3. Thus on this age scale, the colder SST intervals coincident with HE are characterized by lower $\delta^{15}\text{N}$ values, i.e. lower denitrification rates. The correspondence is, however, not as tight, in particular for H3 and H5.

5.2. Scenario 1 – mechanisms

The coincidence of cooler SST and higher organic carbon content would suggest that stronger upwelling of cold nutrient-rich thermocline waters is the prime driving mechanism, regardless of the age scale. Stronger wind-driven equatorial upwelling during Heinrich Events (as suggested by this scenario), however, would be difficult to reconcile with the southern location of the ITCZ reconstructed for these intervals (see Section 2) (Benway et al., 2006; Kienast et al., 2006a; Leduc et al., 2007). The speleothem $\delta^{18}\text{O}$ record from the Caverna Botuvera in southern Brazil (Fig. 1a – site 2) (Wang et al., 2007) as well as travertine deposits from NE Brazil (Wang et al., 2004) strongly support the marine records of a southward shift of the ITCZ during HE (Fig. 5), most notably during H1 and H4. We note that the presence of the Andes may decouple the Brazilian terrestrial ITCZ from the EEP oceanic ITCZ (Takahashi and Battisti, 2007); nevertheless, the coincidence of a strong imprint of H1 and H4 in both locations (on this age scale) would support a common atmospheric forcing. The colder and more nutrient-rich surface waters could be reconciled with a southward position of the ITCZ if they result from faster rates of subsurface circulation (i.e. the speed of the EUC, as opposed to wind-driven upwelling) or enhanced coastal or open ocean

upwelling off Central America and subsequent advection to the Cold Tongue. In the latter case, however, we would expect heavier $\delta^{15}\text{N}$ values reflecting the progressive consumption of nitrate during advection from the coastal centre of upwelling, which we do not observe.

The reduced denitrification rates observed during the intervals of colder SST and higher productivity in the EEP (i.e. HE in this scenario) suggest that ventilation rates (O₂ supply) exerted a dominant control on denitrification in the eastern Pacific OMZ, as suggested in previous studies (Kienast et al., 2002; Higginson and Altabet, 2004; Robinson et al., 2007). Thus, it seems that a mechanism implying enhanced subsurface circulation during HE/AWE, leading to a higher delivery of nutrients and O₂ to the EEP, could explain the multiple observations made for scenario 1.

Models have shown that in response to North Atlantic freshwater forcing as occurs during HE, a deeper thermocline than during the LGM is established over the western and central tropical Pacific, with a slight shoaling over the eastern tropical Pacific (Merkel et al., 2010). The overall steepening of the thermocline increases the speed of the EUC (Bush and Philander, 1999; Andreasen et al., 2001), which in turn should increase O₂ advection into the OMZ and thereby reduce denitrification. Fig. 1b clearly shows the tongue of elevated oxygen located at the equator at 200 m water depth.

Processes in the Southern Ocean where SAMW forms could contribute to the enhanced equatorial circulation. Virtually all water column denitrification takes place in waters in the density range $\sigma = 26.3\text{--}27.2$ that are laterally ventilated by mode and intermediate waters formed at high latitudes (Russell and Dickson, 2003). The most important of these are the intimately linked Sub-Antarctic Mode Water and Antarctic Intermediate Water (SAMW–AAIW) (Sloyan and Rintoul, 2001). Thus SAMW–AAIW is the single most important global source of O₂ to the thermocline (Russell and Dickson, 2003).

Recent work suggests that a colder North Atlantic during HE caused not only the southward shift of the ITCZ/trade winds, but also shifted the Southern Hemisphere westerlies towards the south pole (Anderson et al., 2009; Toggweiler and Lea, 2010). This poleward shift of the westerlies over the Antarctic Circumpolar Current is assumed to spin up the overturning circulation in the Southern Ocean and draw mid-depth water up to the surface around Antarctica (Toggweiler et al., 2006). An intensified overturning

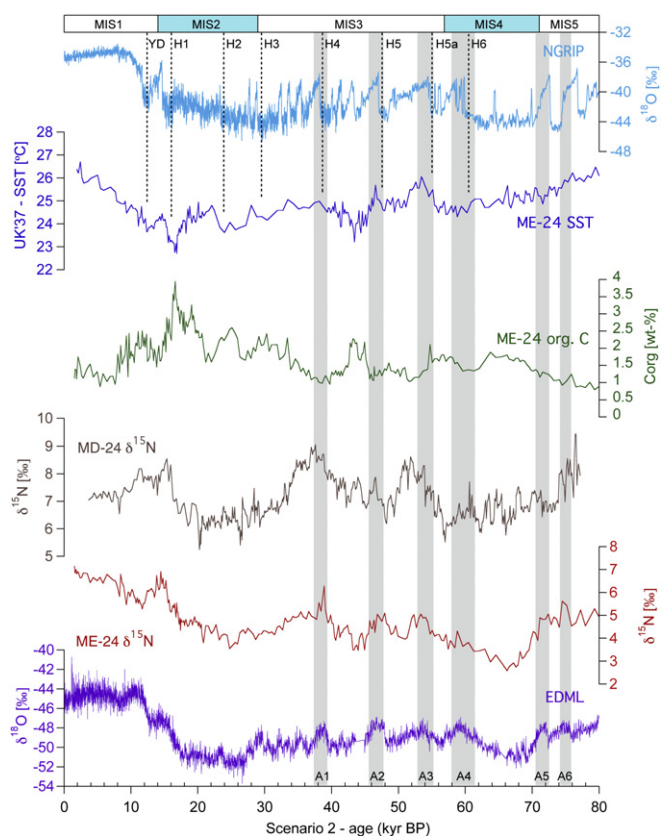


Fig. 7. Multi proxy record of SST, $\delta^{15}\text{N}$ and organic carbon from core ME0005A-24JC, plotted on the age scale obtained with scenario 2 (see Section 5.3 in the text). The $\delta^{15}\text{N}$ record from Nicaragua Basin core MD02-2024 (Pichevin et al., 2010) is shown in brown. Shown for comparison the $\delta^{18}\text{O}$ records from NGRIP (light blue, Greenland ice core) and EDML (purple, Antarctica ice core). Shaded areas represent Antarctic Warm Events (A1–A6). Dotted lines indicate the Younger Dryas (YD) and the Heinrich Events (H1–H6). The Marine Isotopic Stages (MIS) are indicated by the blue and white rectangles at the top (For interpretation of the references to colour in this figure legend, the reader is referred to the web version of this article).

circulation in the Southern Ocean would contribute to the increased supply of oxygen to lower latitude subsurface waters (c.f. Galbraith et al., 2004). Modeling studies of the thermohaline circulation also suggest a close link between the formation of NADW and AAIW, with an intensification of the AAIW circulation cell at times when NADW does not form, and vice versa (Saenko et al., 2003, and references therein). In line with this hypothesis, benthic $\delta^{13}\text{C}$ records from the Southwest Pacific suggest that periods of sudden increases in intermediate and mode water formation occur during AWE/HE, implying an intensified thermocline circulation (Fig. 1a – site 15) (Pahnke and Zahn, 2005). Algal biomarkers from the same location document concurrent periods of increased productivity (Sachs and Anderson, 2005). In the northern Indian Ocean, Jung et al. (2010) also suggest periodic intensification of AAIW flow coeval with HE based on benthic $\delta^{13}\text{C}$.

Fig. 6a presents a schematic illustration of the processes that would be occurring in this first scenario. While this mechanism parsimoniously explains SST and primary productivity variations in the EEP on this age scale, it contradicts previous studies from the Eastern Pacific that show a coherent timing of Antarctic climate change and denitrification (e.g. De Pol-Holz et al., 2007; Robinson et al., 2007; Pichevin et al., 2010). For instance, trace metal records from the Eastern South Pacific suggest a more oxygenated and vertically extended AAIW mass off Chile during the LGM, or in other words that cold stages are characterized by higher AAIW oxygen content (Muratli et al., 2010).

5.3. Scenario 2 – chronology and implications

The second scenario we investigate is based on the assumption that changes in EEP sedimentary $\delta^{15}\text{N}$ followed a Southern Hemisphere forcing, with denitrification peaks in-phase with AWE (De Pol-Holz et al., 2007; Robinson et al., 2007). In Scenario 2, we match the millennial-scale peaks in the $\delta^{15}\text{N}$ record of ME0005A-24JC with the AWE observed in the EDML $\delta^{18}\text{O}_{\text{ice}}$ record (Table 3). Fig. 7 presents the multiple proxy records of ME0005A-24JC plotted on this second age-scale. In this scenario, we do not include the opal data, assuming opal represents only a preservation signal during the burial peak (Dubois et al., in press).

In this case, the millennial-scale warmings recorded in the alkenone SST reconstruction coincide with AWE, in particular A2 and A3. However, the colder intervals do not always match HEs. The coldest interval in MIS3 occurs between H4 and H5. This scenario thus does not support the hypothesis of a North Atlantic derived climate forcing of SST changes in the equatorial Cold Tongue, but rather a coherence with Southern Hemisphere temperatures, as suggested in longer timescale studies (Lea, 2004; Benway et al., 2006; Lea et al., 2006; Mix, 2006; Pena et al., 2008).

On this age model, the organic carbon record reveals minima synchronous with the AWE, and maxima during colder periods in Antarctica (Antarctic stadials, MIS 2 and MIS4).

The record of core MD02-2524 from the Nicaraguan margin (Pichevin et al., 2010) is shown for comparison in Fig. 7. Although the longer timescale variations in the $\delta^{15}\text{N}$ from the two records are quite different, millennial-scale peaks in denitrification appear synchronous on this age scale, in particular during A1, A3 and A6. Because of the strong imprint of local hydrographic changes on the $\delta^{15}\text{N}$ records of the southern boundary of the ETSP OMZ (see Fig. 4 by Robinson et al., 2007), comparison to our EEP records would be less straightforward and thus we do not show these records here.

5.4. Scenario 2 – mechanisms

Scenario 2 is consistent with the more commonly accepted view that lower temperatures of Southern Ocean surface waters increase the physical supply of oxygen and therefore decrease water column denitrification (e.g. Galbraith et al., 2004; Meissner et al., 2005). We note, however, that this mechanism was mostly investigated on orbital timescales: lower glacial-stage sea surface temperature increased oxygen solubility, while stronger winds in high-latitude regions enhanced the rate of thermocline ventilation (Galbraith et al., 2004; Muratli et al., 2010). Translating this mechanism into millennial timescales, previous studies in the ETNP and ETSP OMZ have suggested that a more sluggish circulation of warmer, less oxygen rich thermocline waters during AWE caused the expansion of the ETSP denitrification zone (Robinson et al., 2007; Pichevin et al., 2010). The warmer intervals (i.e. interglacials or AWE in this case) are associated with weaker winds in the Southern Hemisphere, which reduces Ekman convergence and the formation of SAMW-AAIW, thus decreasing the flow rates within the thermocline (Galbraith et al., 2004; Meissner et al., 2005). Fig. 6b presents a schematic illustration of the processes that would be occurring in this second scenario.

The warmer temperatures of thermocline waters would be supported by the warm SST observed during AWE in this scenario (Fig. 7). On the other hand, the strong cooling observed around 44 kyr BP would remain unexplained so far, as it does not coincide with a particular cool interval in either of the polar ice cores.

A more sluggish circulation during AWE would be in line with the observation of lower organic carbon content (i.e. productivity) in the EEP on this age scale. A slower rate of thermocline nutrient delivery, possibly accompanied by a lower preformed nutrient

content, due to reduced upwelling of nutrient rich deep waters around Antarctica, would limit surface productivity in the EEP.

5.5. Broader implications

5.5.1. Ventilation versus consumption

The EEP sedimentary records presented here indicate lower organic carbon content during times of heavier $\delta^{15}\text{N}$ on a millennial timescale, suggesting that variations in suboxia in the ETSP OMZ are not controlled by oxygen demand upstream, at least in the ECT environment. As highlighted in Section 4.2, the organic carbon record of ME0005A-24JC is very similar to that of ME0005A-27JC and TR163-31P, reflecting coherent regional variability (Fig. 2). Thus, during MIS2–4, changes in nutrient delivery and productivity in the EEP upwelling systems do not control the strength of water-column denitrification within the adjacent OMZs as suggested for the deglaciation (Martinez and Robinson, 2010).

Although the mechanisms operating during millennial scale events may be similar to what occurs during the deglaciation, there are fundamental differences. In particular, the deglacial warming shifted the southern hemisphere westerlies to a permanent poleward position leading to the non-stop upwelling of deep, nutrient and CO_2 -rich water masses in the Southern Ocean (Toggweiler et al., 2006; Anderson et al., 2009). The subsequent delivery of these nutrients to the low latitudes produced a significant increase in productivity (Kienast et al., 2006a; Martinez and Robinson, 2010). As suggested by Robinson et al. (2009), the phytoplankton community was not, however, able to keep up with the delivery and relative nutrient utilization decreased. The fundamental difference from the millennial-scale MIS3 events resides in the fact that the deglacial increase in nutrient delivery and productivity was large enough to counter the increased supply in oxygen. The increase in oxygen consumption reduced subsurface oxygen levels, thereby expanding the OMZ and increasing denitrification rates (Martinez and Robinson, 2010). In contrast, the millennial-scale intervals of increased productivity during MIS3 were associated with lower denitrification rates and no significant changes in relative nutrient utilization. Thus we suggest that during MIS3 the physical processes that control intermediate water transport of oxygen dominated over biological processes consuming it.

5.5.2. The Southern Ocean

In summary, the source of discrepancy between the two scenarios investigated here appears to reside in the Southern Ocean and its influence on the thermocline tunneling of oxygen and nutrients. The flux of dissolved oxygen within the permanent thermocline depends on the combined effects of the temperature dependence of oxygen solubility and the vigor of thermocline ventilation. All of these factors are linked to the sea surface conditions in the high-latitude source areas where the thermocline is ventilated (Luyten et al., 1983). The solubility of O_2 in seawater is strongly dependent on temperature, with solubility increasing rapidly as the temperature nears the freezing point. At the same time, the degree of O_2 saturation is dependent on the efficiency of wind mixing in the formation region.

In the case of nutrients, their supply to EEP surface waters will depend on the vigor of subsurface circulation and on the preformed nutrient content. The nutrient content of SAMW/AAIW will depend on the rate of upwelling of deep nutrient-rich water south of the Antarctic Polar Front and the drawdown in nutrients resulting from local productivity while these water masses advect northward at the surface before subducting in the sub-Antarctic Front region. We note that waters from the Northern Hemisphere contribute to the formation of the EUC in the western Pacific (Dugdale et al., 2002),

but here we assume that the relative contribution from northern and southern sourced water did not change significantly.

The first scenario implies that the vigor of thermocline circulation/ventilation dominates over the influence of temperature on O_2 solubility, since O_2 supply to the OMZ on this age scale is enhanced during warm events. AWE correspond to relatively small increases in surface air temperature (3–4 °C, EPICA, 2006), thus the accelerated formation of SAMW-AAIW suggested by paleoceanographic (Pahnke and Zahn, 2005; Anderson et al., 2009) and modeling (Saenko et al., 2003) studies and the faster EUC (Merkel et al., 2010) could compensate the decreased solubility and enhance the O_2 supply to the thermocline by increasing flow rates. Enhanced subsurface circulation during AWE is supported by synchronous increases in productivity (organic carbon).

The second scenario on the other hand implies a dominant control of Southern Ocean SST on the formation and properties of intermediate and mode waters and the resulting supply of O_2 to the OMZ. The lower productivity rates coincident with AWE in this scenario would suggest that these were intervals of more sluggish thermocline circulation and reduced overturning in the Southern Ocean.

5.5.3. Atmospheric nitrous oxide

The increase in atmospheric nitrous oxide (N_2O) concentrations observed in ice cores during D–O warm events appear to lend some support to scenario 1 (Flueckiger et al., 1999; Spahni et al., 2005; Schilt et al., 2009). N_2O is a by-product of denitrification, and a potent greenhouse gas. Scenario 1 suggests reduced denitrification (i.e. smaller oceanic source of atmospheric N_2O) during the coldest stadials. Current estimates of N_2O emissions indicate the modern oceanic contribution to be 10–40% of global production (Khalil and Rasmussen, 1992; Nevison et al., 1995; Bange et al., 1996). As denitrification within the OMZs varied in the past, it probably affected the atmospheric N_2O levels. However, higher rates of denitrification do not necessarily translate directly into higher atmospheric N_2O , because there must be contact between the subsurface water masses and the surface in order for N_2O to be released. Thus the atmospheric N_2O variations could be reflecting terrestrial N_2O production only, which is dominated by northern-hemisphere sources.

6. Conclusion

An increasing number of low-latitude paleoceanographic records demonstrate that the tropical Pacific Ocean underwent substantial biophysical changes on millennial time scales over the past 100,000 yr. The timing of these millennial-scale changes in the EEP and their relation to northern or southern polar climate can provide important constraints on the mechanisms linking the tropical Pacific with high-latitude and global climate changes.

We have used new high-resolution multi-proxy sedimentary records to investigate various mechanisms suggested to control oceanic variability in the EEP. The covariation of nitrogen isotopic records across the EEP during MIS2–4 suggests that changes in denitrification in the nearby OMZ dominated over changes in the degree of nitrate consumption during the last glacial stage. The anti-correlation of the organic carbon records with the nitrogen isotopic records on millennial timescales implies that the changes in denitrification were not caused by higher productivity and oxygen demand in the Cold Tongue upwelling systems, but by changes in thermocline ventilation.

Our study investigates two contrasting scenarios of thermocline ventilation and nutrient delivery in the EEP. Both support the paradigm that reorganizations of intermediate and mode water circulation directly link the EEP to Antarctic climatic change, and

that Southern Ocean dynamics have a dominant control on millennial-scale biogeochemical fluctuations in the Eastern Pacific.

Scenario 1 is consistent with the suggestion that during Heinrich Events/Antarctic Warm Events, the shutdown of deep water formation in the North Atlantic increased overturning circulation in the Southern Ocean. This resulted in an increased supply of nutrients and oxygen to the EEP via SAMW formation and its spreading to the low latitudes. Scenario 2 on the other hand is consistent with the suggestion that variations in denitrification in the Eastern Pacific OMZ follow Antarctic temperature, i.e. that temperature-related O_2 solubility in the region of mode water formation exerts a dominant control on denitrification rates.

Variations in UK-SST appear to be somewhat decoupled from the biogeochemical adjustments. In the case of scenario 1, SST variations agree with a North Atlantic derived climate forcing. The AWE coincide with cooler intervals, as recorded in Greenland ice and North Atlantic sediment cores. An atmospheric bridge from the Atlantic to the Pacific via trade wind forcing could be responsible for the colder surface temperatures in the EEP. In the case of scenario 2, some of the AWE coincide with warmer SST, suggesting the advection of warmer waters within the thermocline.

Although the results of this study cannot discriminate between the two scenarios investigated, it highlights the need to better constrain the changes in overturning circulation in the Southern Ocean, in particular during the millennial scale climatic oscillations. In addition, we suggest that the relative influence of preformed oxygen content and thermocline flow rates on the extent of OMZs and rate of denitrification need to be better constrained.

Acknowledgments

Core material was kindly and generously provided by the Core Repositories of Oregon State University (supported by NSF grant OCE97-12024) and the University of Rhode Island (supported by NSF grant OCE-9102410). We gratefully acknowledge K. Gordon (UBC) for $\delta^{15}N$ analysis, A. Belanger and C. MacMaster (Dalhousie) for laboratory assistance and S. Higginson and K. Thompson (Dalhousie) for their help with statistical treatment. This contribution benefitted from constructive comments of three reviewers, and from discussion with R. Anderson, E. Galbraith and R. Robinson. This work was supported by NSERC Canada (M.K. S.K., S.E.C.), NSF (grant AGS-0602395 for A.C.M.; grant OCE-0318081 for T.D.H.), the Canadian Institute for Advanced Research (CIFAR; M.K.), the Canadian Foundation for Climate and Atmospheric Sciences (CFCAS, S.E.C.), the Geological Society of America (GSA; N.D.) and the Swiss NSF (SNSF grant PBSKP2-128454 for N.D.).

References

- Alley, R.B., Clark, P.U., 1999. The deglaciation of the northern hemisphere: a global perspective. *Annual Review of Earth Planetary Science* 27, 149–182.
- Altabet, M.A., 2001. Nitrogen isotopic evidence for micronutrient control of fractional NO_3^- utilization in the equatorial Pacific. *Limnology and Oceanography* 46, 368–380.
- Altabet, M.A., Francois, R., 1994. Sedimentary nitrogen isotopic ratio as a recorder for surface ocean nitrate utilization. *Global Biogeochemical Cycles* 8, 103–116.
- Anderson, R.F., Ali, S., Bradtmiller, L.I., Nielsen, S.H.H., Fleisher, M.Q., Anderson, B.E., Burckle, L.H., 2009. Wind-driven upwelling in the southern ocean and the deglacial rise in atmospheric CO_2 . *Science* 323, 1443–1448.
- Andreasen, D.H., Ravelo, A.C., Broccoli, A.J., 2001. Remote forcing at the Last Glacial Maximum in the Tropical Pacific Ocean. *Journal of Geophysical Research* 106, 879–897.
- Antoine, D., Andre, J.M., Morel, A., 1996. Oceanic primary production: 2. Estimation at global scale from satellite (coastal zone color scanner) chlorophyll. *Global Biogeochemical Cycles* 10, 57–69.
- Bange, H.W., Rapsomanikis, S., Andreae, M.O., 1996. Nitrous oxide in coastal waters. *Global Biogeochemical Cycles* 10, 197–207.
- Benway, H.M., Mix, A.C., 2004. Oxygen isotopes, upper-ocean salinity, and precipitation sources in the Eastern Tropical Pacific. *Earth and Planetary Science Letters* 224, 493–507.
- Benway, H.M., Mix, A.C., Haley, B.A., Klinkhammer, G.P., 2006. Eastern Pacific warm pool paleosalinity and climate variability: 0–30 kyr. *Paleoceanography* 21, PA3008.
- Blunier, T., Brook, E.J., 2001. Timing of millennial-scale climate change in Antarctica and Greenland during the last glacial period. *Science* 291, 109–112.
- Broecker, W.S., Petzet, D.M., Rind, D., 1985. Does the ocean-atmosphere system have more than one stable mode of operation? *Nature* 315, 21–26.
- Bush, A.B.G., Philander, S.G.H., 1999. The climate of the Last Glacial Maximum: results from a coupled atmosphere-ocean general circulation model. *Journal of Geophysical Research* 104, 5249–5255.
- Cane, M.A., 1998. A role for the tropical Pacific. *Science* 282, 59–61.
- Chai, F., Lindley, S.T., Barber, R.T., 1996. Origin and maintenance of a high nitrate condition in the equatorial Pacific. *Deep-Sea Research II* 43, 1031–1064.
- Charles, C.D., Froehlich, P.N., Zibello, M.A., Mortlock, R.A., Morley, J.J., 1991. Biogenic opal in Southern Ocean sediments over the last 450,000 years: implications for surface water chemistry and circulation. *Paleoceanography* 6, 697–728.
- Chavez, F.P., Barber, R.T., 1987. An estimate of new production in the equatorial Pacific. *Deep-Sea Research* 34, 1229–1243.
- De Pol-Holz, R., Ulloa, O., Dezileau, L., Kaiser, J., Lamy, F., Hebbeln, D., 2006. Melting of the Patagonian Ice Sheet and deglacial perturbations of the nitrogen cycle in the eastern South Pacific. *Geophysical Research Letters* 33, L04704.
- De Pol-Holz, R., Ulloa, O., Lamy, F., Dezileau, L., Sabatier, P., Hebbeln, D., 2007. Late Quaternary variability of sedimentary nitrogen isotopes in the eastern South Pacific Ocean. *Paleoceanography* 22, PA2207.
- Drexler, J.W., Rose, W.I.J., Sparks, R.S.J., Ledbetter, M.T., 1980. The Los Chocoyos Ash, Guatemala: a major stratigraphic marker in middle America and in three ocean basins. *Quaternary Research* 13, 327–345.
- Dubois, N., Kienast, M., Normandeau, C., Herbert, T.D., 2009. The east equatorial Pacific cold tongue during the last glacial maximum as seen from alkenone paleothermometry. *Paleoceanography* 24, PA4207.
- Dubois, N., Kienast, M., Kienast, S.S., Calvert, S.E., Francois, R., Anderson, R.F. Sedimentary opal records in the Eastern Equatorial Pacific: It's not all about leakage. *Global Biogeochemical Cycles*, 2010GB003821, in press.
- Dubois, N., Kienast, M., Kienast, S.S., Calvert, S.E. Diverging glacial-interglacial nutrient regimes in the eastern tropical Pacific during the last 150 kyr, in preparation.
- Dugdale, R.C., Wischmeyer, A.G., Wilkerson, F.P., Barber, R.T., Chai, F., Jiang, M.S., Peng, T.H., 2002. Meridional asymmetry of surface nutrients to the equatorial Pacific upwelling ecosystem and its potential impact on ocean-atmosphere CO_2 flux; a data and modeling approach. *Deep-Sea Research II* 49, 2513–2531.
- Dugdale, R.C., Lyle, M., Wilkerson, F.P., Chai, F., Barber, R.T., Peng, T.H., 2004. Influence of equatorial diatom processes on Si deposition and atmospheric CO_2 cycles at glacial/interglacial timescales. *Paleoceanography* 19, PA3011.
- EPICA Community Members, 2006. One-to-one coupling of glacial climate variability in Greenland and Antarctica. *Nature* 444, 195–198.
- Emmer, E., Thunell, R.C., 2000. Nitrogen isotope variations in Santa Barbara Basin sediments: implications for denitrification in the eastern tropical North Pacific during the last 50,000 years. *Paleoceanography* 15, 377–387.
- Faibanks, R.G., Mortlock, R.A., Chiu, T.C., Cao, L., Kaplan, A., Guilderson, T.P., Fairbanks, T.W., Bloom, A.L., Grootes, P.M., Nadeau, M.J., 2005. Radiocarbon calibration curve spanning 0 to 50,000 years BP based on paired ^{230}Th / ^{234}U / ^{238}U and ^{14}C dates on pristine corals. *Quaternary Science Reviews* 24, 1781–1796.
- Farrell, J.W., Pedersen, T.F., Calvert, S.E., Nielsen, B., 1995. Glacial-interglacial changes in nutrient utilization in the equatorial Pacific Ocean. *Nature* 377, 514–517.
- Feldberg, M.J., Mix, A.C., 2002. Sea-surface temperature estimates in the southeast Pacific based on planktonic foraminiferal species: modern calibration and Last Glacial Maximum. *Marine Micropaleontology* 44, 1–29.
- Feldberg, M.J., Mix, A.C., 2003. Planktonic foraminifera, sea-surface temperatures, and mechanisms of oceanic change in the Peru and south Equatorial Currents, 0–150 ka BP. *Paleoceanography* 18, 1016.
- Fitzwater, S.E., Coale, K.H., Gordon, R.M., Johnson, K.S., Ondrusek, M.E., 1996. Iron deficiency and phytoplankton growth in the equatorial Pacific. *Deep-Sea Research II* 43, 995–1015.
- Flueckiger, J., Daellenbach, A., Blunier, T., Stauffer, B., Stocker, T.F., Raynaud, D., Barnola, J.M., 1999. Variations in atmospheric N_2O concentration during abrupt climatic changes. *Science* 285, 227–230.
- Galbraith, E.D., Kienast, M., Pedersen, T.F., Calvert, S.E., 2004. Glacial-interglacial modulation of the marine nitrogen cycle by high-latitude O_2 supply to the global thermocline. *Paleoceanography* 19, PA4007.
- Ganeshram, R.S., Pedersen, T.F., 1998. Glacial-interglacial variability in upwelling and bioproductivity off NW Mexico: implications for Quaternary paleoclimate. *Paleoceanography* 13, 634–645.
- Ganeshram, R.S., Pedersen, T.F., Calvert, S.E., McNeill, G.W., Fontugne, M.R., 2000. Glacial-interglacial variability in denitrification in the world's oceans: causes and consequences. *Paleoceanography* 15, 361–376.
- Garcia, H.E., Locarnini, R.A., Boyer, T.P., Antonov, J.I., 2006a. World Ocean Atlas 2005, vol. 4: Nutrients (Phosphate, Nitrate, Silicate). In: NOAA Atlas NESDIS, vol. 64. U.S. Government Printing Office, Washington, DC, 396 pp.
- Garcia, H.E., Locarnini, R.A., Boyer, T.P., Antonov, J.I., 2006b. World Ocean Atlas 2005, vol. 3: Dissolved Oxygen, Apparent Oxygen Utilization, and Oxygen Saturation. In: NOAA Atlas NESDIS, vol. 63. U.S. Government Printing Office, Washington, DC, 342 pp.
- Gherardi, J.M., Labeyrie, L., McManus, J.F., Francois, R., Skinner, L.C., Cortijo, E., 2005. Evidence from the northeastern Atlantic basin for variability in the rate of the meridional overturning circulation through the last deglaciation. *Earth and Planetary Science Letters* 240, 710–723.

- Hemming, S., 2004. Heinrich events: massive late Pleistocene detritus layers of the north Atlantic and their global climate imprint. *Reviews of Geophysics* 42, RG1005.
- Hendy, I.L., Pedersen, T.F., 2006. Oxygen minimum zone expansion in the eastern tropical north Pacific during deglaciation. *Geophysical Research Letters* 33, L20602.
- Hendy, I.L., Pedersen, T.F., Kennett, J.P., Tada, R., 2004. Intermittent existence of a southern Californian upwelling cell during submillennial climate change of the last 60 kyr. *Paleoceanography* 19, PA3007.
- Herbert, T.D., Schuffert, J.D., Thomas, D., Lange, C.B., Weinheimer, A., Peleo-Alampay, A., 1998. Depth and seasonality of alkenone production along the California margin inferred from a core top transect. *Paleoceanography* 13, 263–271.
- Higginson, M.J., Altabet, M.A., 2004. Initial test of the silicic acid leakage hypothesis using sedimentary biomarkers. *Geophysical Research Letters* 31, L18303.
- Hostetler, S., Pisias, N., Mix, A.C., 2006. Sensitivity of Last Glacial maximum climate to uncertainties in tropical and subtropical ocean temperatures. *Quaternary Science Reviews* 25, 1168–1185.
- Hughen, K.A., Baillie, M.G.L., Bard, E., Beck, J.W., Bertrand, C.J.H., Blackwell, P.G., Buck, C.E., Burr, G.S., Cutler, K.B., Damon, P.E., Edwards, R.L., Fairbanks, R.G., Friedrich, M., Guilderson, T.P., Kromer, B., McCormac, G., Manning, S., Ramsey, C.B., Reimer, P.J., Reimer, R.W., Remmele, S., Southon, J.R., Stuiver, M., Talamo, S., Taylor, F.W., van der Plicht, J., Weyhenmeyer, C.E., 2004. Marine04 Marine radiocarbon age calibration, 26–0 ka BP. *Radiocarbon* 46, 1059–1086.
- Jung, S.J.A., Kroon, D., Ganssen, G., Peeters, F., Ganeshram, R., 2010. Southern hemisphere intermediate water formation and the bi-polar seesaw. *PAGES News* 18, 36–38.
- Khalil, M.A.K., Rasmussen, R.A., 1992. The global sources of nitrous oxide. *Journal of Geophysical Research* 97, 14651–14660.
- Kienast, S.S., Calvert, S.E., Pedersen, T.F., 2002. Nitrogen isotope and productivity variations along the northeast Pacific margin over the last 120 kyr: surface and subsurface paleoceanography. *Paleoceanography* 17, 1055.
- Kienast, M., Kienast, S.S., Calvert, S.E., Eglinton, T.I., Mollenhauer, G., Francois, R., Mix, A.C., 2006a. Eastern Pacific cooling and Atlantic overturning circulation during the last deglaciation. *Nature* 443, 846–849.
- Kienast, S.S., Kienast, M., Jaccard, S., Calvert, S.E., Francois, R., 2006b. Testing the silica leakage hypothesis with sedimentary opal records from the eastern equatorial Pacific over the last 150 kyr. *Geophysical Research Letters* 33, L15607.
- Kienast, S.S., Kienast, M., Mix, A.C., Calvert, S.E., Francois, R., 2007. Thorium-230 normalized particle flux and sediment focusing in the Panama basin region during the last 30,000 years. *Paleoceanography* 22, PA2213.
- Koutavas, A., Sachs, J.P., 2008. Northern timing of deglaciation in the eastern equatorial Pacific from alkenone paleothermometry. *Paleoceanography* 23, PA4205.
- Kusch, S., Eglinton, T.I., Mix, A.C., Mollenhauer, G., 2010. Timescales of lateral sediment transport in the Panama basin as revealed by radiocarbon ages of alkenones, total organic carbon and foraminifera. *Earth and Planetary Science Letters* 290, 340–350.
- Lea, D.W., 2004. The 100,000-yr cycle in tropical SST, greenhouse forcing and climate sensitivity. *Journal of Climate* 17, 2170–2179.
- Lea, D.W., Pak, D.K., Spero, H.J., 2000. Climate impact of late quaternary equatorial Pacific sea surface temperature variations. *Science* 289, 1719–1724.
- Lea, D.W., Pak, D.K., Belanger, C.L., Spero, H.J., Hall, M.A., Shackleton, N.J., 2006. Paleoclimate history of Galapagos surface waters over the last 135,000 yr. *Quaternary Science Reviews* 25, 1152–1167.
- Leduc, G., Vidal, L., Tachikawa, K., Rostek, F., Sonzogni, C., Beaufort, L., Bard, E., 2007. Moisture transport across central America as a positive feedback on abrupt climatic changes. *Nature* 445, 908–911.
- Lisiecki, L.E., Raymo, M.E., 2009. Diachronous benthic $\delta^{18}\text{O}$ responses during late Pleistocene terminations. *Paleoceanography* 24, PA3210.
- Liu, Z., Yang, H., 2003. Extratropical control of tropical climate, the atmospheric bridge and oceanic tunnel. *Geophysical Research Letters* 30, 1230.
- Locarnini, R.A., Mishonov, A.V., Antonov, J.I., Boyer, T.P., Garcia, H.E., 2006. World Ocean Atlas 2005, vol. 1, Temperature. In: NOAA Atlas NESDIS, vol. 61. NOAA, Silver Spring, MD, 182 pp.
- Loubere, P., 2002. Remote vs. local control of changes in eastern equatorial Pacific bioproductivity from the Last Glacial Maximum to the present. *Global and Planetary Change* 35, 113–126.
- Luyten, J.R., Pedlosky, J., Stommel, H., 1983. The ventilated thermocline. *Journal of Physical Oceanography* 13, 292–309.
- Lyle, M., Mix, A.C., Pisias, N.G., 2002. Patterns of CaCO_3 deposition in the eastern tropical Pacific Ocean for the last 150 kyr: evidence for a southeast Pacific depositional spike during marine isotope stage (MIS) 2. *Paleoceanography* 17, 1013.
- Martin, J.H., Gordon, R.M., Fitzwater, S.E., 1991. The case for iron. *Limnology and Oceanography* 36, 1793–1802.
- Martinez, P., Robinson, R.S., 2010. Increase in water column denitrification during the last deglaciation: the influence of oxygen demand in the eastern equatorial Pacific. *Biogeosciences* 7, 1–9.
- Martinez, P., Lamy, F., Robinson, R.S., Pichevin, L.E., Billy, I., 2006. Atypical $\delta^{15}\text{N}$ variations at the southern boundary of the East Pacific oxygen minimum zone over the last 50 ka. *Quaternary Science Reviews* 25, 3017–3028.
- McManus, J.F., Francois, R., Gherardi, J.M., Keigwin, L.D., Brown-Leger, S., 2004. Collapse and rapid resumption of Atlantic meridional circulation linked to deglacial climate changes. *Nature* 428, 834–837.
- Meissner, K.J., Galbraith, E.D., Voelker, C., 2005. Denitrification under glacial and interglacial conditions: a physical approach. *Paleoceanography* 20, PA3001.
- Merkel, U., Prange, M., Schulz, M., 2010. ENSO variability and teleconnections during glacial climates. *Quaternary Science Reviews* 29, 86–100.
- Mitchell, T.P., Wallace, J.M., 1992. The annual cycle in equatorial convection and sea surface temperature. *Journal of Climate* 5, 1140–1156.
- Mix, A.C., 2006. Running hot and cold in the eastern equatorial Pacific. *Quaternary Science Reviews* 25, 1147–1149.
- Mix, A.C., Morey, A.E., Pisias, N.G., Hostetler, S.W., 1999. Foraminiferal faunal estimates of paleotemperature: circumventing the no-analog problem yields cool ice-age tropics. *Paleoceanography* 14, 350–359.
- Mortlock, R.A., Froehlich, P.N., 1989. A simple method for the rapid determination of biogenic opal in pelagic marine sediments. *Deep-Sea Research* 36, 1415–1426.
- Muratli, J.M., Chase, Z., Mix, A.C., McManus, J., 2010. Increased ice-age influence of the Chilean Margin by Antarctic Intermediate Water. *Nature Geosciences* 3, 23–26.
- Nevison, C.D., Weiss, R.F., Erickson, D.J.I., 1995. Global oceanic emissions of nitrous oxide. *Journal of Geophysical Research* 100, 15,809–15,820.
- Pahnke, K., Zahn, R., 2005. Southern hemisphere water mass conversion linked with north Atlantic climate variability. *Science* 307, 1741–1746.
- Pahnke, K., Sachs, J.P., Keigwin, L.D., Timmermann, A., Shang-Ping, X., 2007. Eastern tropical Pacific hydrologic changes during the past 27,000 years from D/H ratios in alkenones. *Paleoceanography* 22, PA4214.
- Paillard, D., Labeyrie, L., Yiou, P., 1996. Macintosh program performs time-series analysis. *Eos, Transactions, American Geophysical Union* 77, 379.
- Patrick, A., Thunell, R.C., 1997. Tropical Pacific sea surface temperatures and upper water column thermal structure during the last glacial maximum. *Paleoceanography* 12, 649–657.
- Pedersen, T.F., Nielsen, B., Pickering, M., 1991. Timing of late quaternary productivity pulses in the Panama basin and implications for atmospheric CO_2 . *Paleoceanography* 6, 657–677.
- Pena, L.D., Cacho, I., Ferretti, P., Hall, M.A., 2008. El Niño–Southern Oscillation–like variability during glacial terminations and interlatitudinal teleconnections. *Paleoceanography* 23, PA3101.
- Pichevin, L.E., Reynolds, B.C., Ganeshram, R.S., Cacho, I., Pena, L.D., Keefe, K., Ellam, R.M., 2009. Enhanced carbon pump inferred from relaxation of nutrient limitation in the glacial ocean. *Nature* 459, 1114–1118.
- Pichevin, L.E., Ganeshram, R.S., Francavilla, S., Arellano-Torres, E., Pedersen, T.F., Beaufort, L., 2010. Inter-hemispheric leakage of isotopically heavy nitrate in the Eastern Tropical Pacific during the last glacial period. *Paleoceanography* 25, PA1204.
- Pisias, N.G., Mix, A.C., 1997. Spatial and temporal oceanographic variability of the eastern equatorial Pacific during the late Pleistocene: evidence from Radiolaria microfossils. *Paleoceanography* 12, 381–393.
- Prahl, F.G., Muehlhausen, L.A., Zahn, D.L., 1988. Further evaluation of long-chain alkenones as indicators of paleoceanographic conditions. *Geochimica et Cosmochimica Acta* 52, 2303–2310.
- Pride, C., Thunell, R., Sigman, D., Keigwin, L., Altabet, M., 1999. Nitrogen isotopic variations in the Gulf of California since the last deglaciation: response to global climate change. *Paleoceanography* 14, 397–409.
- Raymo, M.E., Ganley, K., Carter, S., Oppo, D.W., McManus, J.F., 1998. Millennial-scale climate instability during the early Pleistocene epoch. *Nature* 392, 699–702.
- Reimer, P.J., Baillie, M.G.L., Bard, E., Bayliss, A., Beck, J.W., Blackwell, P.G., Ramsey, C.B., Buck, C.E., Burr, G.S., Edwards, R.L., Friedrich, M., Grootes, P.M., Guilderson, T.P., Hajdas, I., Heaton, T.J., Hogg, A.G., Hughen, K.A., Kaiser, K.F., Kromer, B., McCormac, F.G., Manning, S.W., Reimer, R.W., Richards, D.A., Southon, J.R., Talamo, S., Turney, C.S.M., van der Plicht, J., Weyhenmeyer, C.E., 2009. Intcal09 and Marine09 radiocarbon age calibration curves, 0–50,000 years cal BP. *Radiocarbon* 51, 1111–1150.
- Robinson, R.S., Mix, A.C., Martinez, P., 2007. Southern Ocean control on the extent of denitrification in the southeast Pacific over the last 70 ka. *Quaternary Science Reviews* 26, 201–212.
- Robinson, R.S., Martinez, P., Pena, L.D., Cacho, I., 2009. Nitrogen isotopic evidence for deglacial changes in nutrient supply in the Eastern Equatorial Pacific. *Paleoceanography* 24, PA4213.
- Rohling, E.J., Liu, Q.S., Roberts, A.P., Stanford, J.D., Rasmussen, S.O., Langen, P.L., Siddall, M., 2009. Controls on the east Asian monsoon during the last glacial cycle, based on comparison between Hulu Cave and polar ice-core records. *Quaternary Science Reviews* 28, 3291–3302.
- Russell, J.L., Dickson, A.G., 2003. Variability in oxygen and nutrients in South Pacific Antarctic Intermediate Water. *Global Biogeochemical Cycles* 17 (2), 1033. doi:10.1029/2000GB001317.
- Sachs, J.P., Anderson, R.F., 2005. Increased productivity in the subantarctic ocean during Heinrich events. *Nature* 434, 1118–1121.
- Saenko, O.A., Weaver, A.J., Gregory, J.M., 2003. On the link between the two modes of the ocean thermohaline circulation and the formation of global-scale water masses. *Journal of Climate* 16, 2797–2801.
- Sarmiento, J.L., Gruber, N., Brzezinski, M.A., Dunne, J.P., 2004. High-latitude controls of thermocline nutrients and low latitude biological productivity. *Nature* 427, 56–60.
- Schilt, A., Baumgartner, M., Blunier, T., Schwander, J., Spahni, R., Fisher, H., Stocker, T.F., 2009. Glacial–interglacial and millennial-scale variations in the atmospheric nitrous oxide concentration during the last 800,000 years. *Quaternary Science Reviews* 22, 182–192.
- Schlitzer, R., 2010. Ocean Data View. <<http://odv.awi.de>>.

- Singer, B.S., Guillou, H., Jicha, B.R., Laj, C., Kissel, C., Beard, B.L., Johnson, C.M., 2009. $^{40}\text{Ar}/^{39}\text{Ar}$, K–Ar and ^{230}Th – ^{238}U dating of the Laschamp excursion: a radioisotopic tie-point for ice core and climate chronologies. *Earth and Planetary Science Letters* 286, 80–88.
- Skinner, L.C., Shackleton, N.J., 2005. An Atlantic lead over Pacific deep-water change across Termination I: implications for the application of the marine isotope stage stratigraphy. *Quaternary Science Reviews* 24, 571–580.
- Sloyan, B.M., Rintoul, S.R., 2001. Circulation, renewal, and modification of Antarctic Mode and Intermediate Water. *Journal of Physical Oceanography* 31, 1005–1030.
- Spahni, R., Chappellaz, J., Stocker, T.F., Loulergue, L., Hausammann, G., Kawamura, K., Flueckiger, J., Schwander, J., Raynaud, D., Masson-Delmotte, V., Jouzel, J., 2005. Atmospheric methane and nitrous oxide of the late Pleistocene from Antarctic ice cores. *Science* 310, 1317–1321.
- Spero, H.J., Lea, D.W., 2002. The cause of carbon isotope minimum events on glacial terminations. *Science* 296, 522–525.
- Stuiver, M., Reimer, P.J., 1993. Extended ^{14}C data base and revised CALIB 3.0 ^{14}C age calibration program. *Radiocarbon* 35, 215–230. <http://radiocarbon.pa.qub.ac.uk/calib/>. Available at.
- Takahashi, K., Battisti, D.S., 2007. Processes controlling the mean tropical Pacific precipitation patten. Part I: the Andes and the Eastern Pacific ITCZ. *Journal of Climate* 20, 3434–3451.
- Takahashi, T., Sutherland, S.C., Sweeney, C., Poisson, A., Metzl, N., Tilbrook, B., Bates, N., Wanninkhof, R., Feely, R.A., Sabine, C.L., Olafsson, J., Nojiri, Y., 2002. Global sea–air CO_2 flux based on climatological surface ocean pCO_2 , and seasonal biological and temperature effects. *Deep-Sea Research II* 49, 1601–1622.
- Thunell, R.C., Kepple, A.B., 2004. Glacial-Holocene $\delta^{15}\text{N}$ record from the Gulf of Tehuantepec, Mexico: implications for denitrification in the eastern equatorial Pacific and changes in atmospheric N_2O . *Global Biogeochemical Cycles* 18, GB1001.
- Toggweiler, J.R., Carson, S.R., 1995. What are upwelling systems contributing to the ocean's carbon and nutrient budgets? In: Summerhayes, C.P., Emeis, K.C., Angel, M.V., Smith, H.J., Zeitzschel, B. (Eds.), *Upwelling in the Ocean: Modern Processes and Ancient Records*. John Wiley & Sons Ltd, pp. 337–360.
- Toggweiler, J.R., Lea, D.W., 2010. Temperature differences between the hemispheres drive Ice-Age climate variability. *Paleoceanography* 25, PA2212.
- Toggweiler, J.R., Dixon, K., Broecker, W.S., 1991. The Peru upwelling and the ventilation of the South Pacific thermocline. *Journal of Geophysical Research* 96, 20467–20497.
- Toggweiler, J.R., Russell, J.L., Carson, S.R., 2006. Midlatitude westerlies, atmospheric CO_2 , and climate change during the ice ages. *Paleoceanography* 21, PA2005.
- Tsuchiya, M., Talley, L.D., 1998. A Pacific hydrographic section at 88°W: water-property distribution. *Journal of Geophysical Research* 103, 12,899–12,918.
- Verardo, D.J., Froehlich, P.N., McIntyre, A., 1990. Determination of organic carbon and nitrogen in marine sediments using the Carlo Erba NA-1500 analyzer. *Deep-Sea Research* 37, 157–165.
- Wang, Y.J., Cheng, H., Edwards, R.L., An, Z.S., Wu, J.Y., Shen, C.C., Dorale, J.A., 2001. A high-resolution absolute-dated late Pleistocene monsoon record from Hulu Cave, China. *Science* 294, 2345–2348.
- Wang, X.F., Auler, A.S., Edwards, R.L., Cheng, H., Cristalli, P.S., Smart, P.L., Richards, D.A., Shen, C.C., 2004. Wet periods in northeastern Brazil over the past 210 kyr linked to distant climate anomalies. *Nature* 432, 740–743.
- Wang, X., Auler, A.S., Edwards, R.L., Cheng, H., Ito, E., Wang, Y.J., Kong, X., Solheid, M., 2007. Millennial-scale precipitation changes in southern Brazil over the past 90,000 years. *Geophysical Research Letters* 34, L23701.
- Zaucker, F., Stocker, T.F., Broecker, W.S., 1994. Atmospheric freshwater fluxes and their effect on the global thermohaline circulation. *Journal of Geophysical Research* 99, 12,443–12,457.
- Zhang, R., Delworth, T.L., 2005. Simulated tropical response to a substantial weakening of the Atlantic thermohaline circulation. *Journal of Climate* 18, 1853–1860.